

AD-A256 184

AD-A256 184

2



TECHNICAL REPORT-RD-WS-92-7

DTIC
ELECTE
SEP 3 1992
S C D



**SPATIAL LIGHT MODULATOR NONLINEARITY EFFECTS
IN OPTICAL PATTERN RECOGNITION ARCHITECTURES**

Tracy D. Hudson
Weapons Sciences Directorate
Research, Development, and Engineering Center

JUNE 1992



U.S. ARMY MISSILE COMMAND

Redstone Arsenal, Alabama 35898-5000

Approved for public release; distribution is unlimited.

92 9 02 088

92-24352



DESTRUCTION NOTICE

FOR CLASSIFIED DOCUMENTS, FOLLOW THE PROCEDURES IN DoD 5200.22-M, INDUSTRIAL SECURITY MANUAL, SECTION II-19 OR DoD 5200.1-R, INFORMATION SECURITY PROGRAM REGULATION, CHAPTER IX. FOR UNCLASSIFIED, LIMITED DOCUMENTS, DESTROY BY ANY METHOD THAT WILL PREVENT DISCLOSURE OF CONTENTS OR RECONSTRUCTION OF THE DOCUMENT.

DISCLAIMER

THE FINDINGS IN THIS REPORT ARE NOT TO BE CONSTRUED AS AN OFFICIAL DEPARTMENT OF THE ARMY POSITION UNLESS SO DESIGNATED BY OTHER AUTHORIZED DOCUMENTS.

TRADE NAMES

USE OF TRADE NAMES OR MANUFACTURERS IN THIS REPORT DOES NOT CONSTITUTE AN OFFICIAL ENDORSEMENT OR APPROVAL OF THE USE OF SUCH COMMERCIAL HARDWARE OR SOFTWARE.

REPORT DOCUMENTATION PAGE			Form Approved OMB No. 0704-0188		
1a. REPORT SECURITY CLASSIFICATION Unclassified		1b. RESTRICTIVE MARKINGS			
2a. SECURITY CLASSIFICATION AUTHORITY		3. DISTRIBUTION/AVAILABILITY OF REPORT <i>Approved for public release; distribution is unlimited.</i>			
2b. DECLASSIFICATION/DOWNGRADING SCHEDULE					
4. PERFORMING ORGANIZATION REPORT NUMBER(S) Technical Report RD-WS-92-7		5. MONITORING ORGANIZATION REPORT NUMBER (S)			
6a. NAME OF PERFORMING ORGANIZATION Weapons Sciences Directorate RD&E Center	6b. OFFICE SYMBOL (if applicable) AMSMI-RD-WS-PO	7a. NAME OF MONITORING ORGANIZATION			
6c. ADDRESS (City, State, and ZIP Code) Commander, U. S. Army Missile Command ATTN: AMSMI-RD-WS-PO Redstone Arsenal, AL 35898-5248		7b. ADDRESS (City, State, and ZIP Code)			
8a. NAME OF FUNDING/SPONSORING ORGANIZATION	8b. OFFICE SYMBOL (if applicable)	9. PROCUREMENT INSTRUMENT IDENTIFICATION NUMBER			
8c. ADDRESS (City, State, and ZIP Code)		10. SOURCE OF FUNDING NUMBERS			
		PROGRAM ELEMENT NO.	PROJECT NO.	TASK NO.	WORK UNIT ACCESSION NO.
11. TITLE (Include Security Classification) SPATIAL LIGHT MODULATOR NONLINEARITY EFFECTS IN OPTICAL PATTERN RECOGNITION ARCHITECTURES					
12. PERSONAL AUTHOR(S) Tracy D. Hudson					
13a. TYPE OF REPORT Final	13b. TIME COVERED FROM <u>Dec 90</u> TO <u>Nov 91</u>	14. DATE OF REPORT (Year, Month, Day) June 1992	15. PAGE COUNT 70		
16. SUPPLEMENTARY NOTATION					
17.	COSATI CODES		18. SUBJECT TERMS (Continue on reverse if necessary and identify by block number)		
FIELD	GROUP	SUB-GROUP	Spatial light modulator; phase modulation; optical correlator; optical processing		
19. ABSTRACT (Continue on reverse if necessary and identify by block number) <p>Spatial Light Modulators (SLMs) are key elements in real-time optical signal processors. The performance limitations of spatial light modulators have significantly hampered the application of optical pattern recognition systems, such as optical correlators, to "real-world" problems. Exploration of nonlinear transformations in the Fourier plane of optical processors, such as correlators, has recently become a topic of considerable interest. Computer simulations of these nonlinear transformations have been extensively reported. The response of several optically addressed SLMs, proposed for use in such nonlinear transformation processes, has not been characterized. The response of several optically addressed SLMs, including the Hughes LCLV, the GEC-Marconi SLM, and optically addressed ferroelectric liquid crystal SLMs from the University of Colorado-Boulder, have been experimentally determined. The response is reported for the candidate SLMs with respect to variations in the driving waveform frequency and amplitude, incident read beam intensity, and spectral variations in the read beam. Furthermore, equivalent circuit models of the candidate SLMs have been developed to explain the response of these modulators. The nonlinear transformation function of the optically addressed SLMs may be utilized to improve the performance of optical processors, such as correlators.</p>					
20. DISTRIBUTION/AVAILABILITY OF ABSTRACT <input type="checkbox"/> UNCLASSIFIED/UNLIMITED <input checked="" type="checkbox"/> SAME AS RPT. <input type="checkbox"/> DTIC USERS		21. ABSTRACT SECURITY CLASSIFICATION Unclassified			
22a. NAME OF RESPONSIBLE INDIVIDUAL Tracy D. Hudson		22b. TELEPHONE (Include Area Code) (205) 876-6242	22c. OFFICE SYMBOL AMSMI-RD-WS-PO		

ACKNOWLEDGEMENTS

The author would like to express his appreciation to Dr. Don A. Gregory, Group Leader of the Photonics & Optical Sciences Group, Weapons Sciences Directorate, RD&E Center, for his invaluable instruction and guidance during the course of this research. The author also wishes to express gratitude to Mr. James C. Kirsch and Mr. David J. Lanteigne of the Weapons Sciences Directorate, for their constant interest and advice. A special thanks to Janine Reardon who spent many hours discussing spatial light modulator operating principles and quirks with me.

DTIC QUALITY INSPECTED 3

iii/(iv blank)

Accession For	
NTIS GRA&I	<input checked="" type="checkbox"/>
DTIC TAB	<input type="checkbox"/>
Unannounced	<input type="checkbox"/>
Justification	
By	
Distribution/	
Availability Codes	
Dist	Avail and/or Special
A-1	

TABLE OF CONTENTS

	<u>Page</u>
I. INTRODUCTION	1
II. PRINCIPLES OF SPATIAL LIGHT MODULATOR (SLM) OPERATION.....	1
A. Liquid Crystal Light Valve (LCLV)	2
B. GEC-Marconi Research SLM	5
C. Optically Addressed Ferroelectric Liquid Crystal SLM	5
III. SLM PERFORMANCE CHARACTERISTICS.....	7
A. Resolution Measurements.....	7
B. Visibility Measurements.....	11
C. Response Time Measurements.....	14
IV. HUGHES LIQUID CRYSTAL LIGHT VALVE (LCLV) NONLINEAR RESPONSE.....	20
A. LCLV Response to 632.8 nm Read Beam Illumination.....	20
B. LCLV Response to 514.5 nm Read Beam Illumination.....	23
V. GEC-MARCONI SLM RESPONSE.....	28
VI. FLC SLM RESPONSE.....	36
VII. EQUIVALENT CIRCUIT MODELS	41
A. Hughes Liquid Crystal Light Valve (LCLV)	41
B. GEC-Marconi SLM.....	45
C. Optically Addressed Ferroelectric Liquid Crystal SLM	46
VIII. CONCLUSION.....	51
REFERENCES	54

LIST OF FIGURES

<u>Figure</u>	<u>Page</u>
1 Schematic of Hughes LCLV	3
2 LCLV Operation with Polarizer/Analyzer Pair	4
3 Elementary Circuit Model of an SLM.....	5
4 Electro-optical Modulation of FLC.....	6
5 SLM Resolution Measurement System	8
6 Resolution Limit of System Shown in Figure 5	8
7 Resolution of the Hughes LCLVs.....	9
8 Resolution of the GEC-Marconi Research SLM.....	10
9 Resolution of the Ferroelectric Liquid Crystal SLMs	13
10 Visibility Measurement System.....	14
11 Response Time Measurement System.....	15
12 Response of (a) the late-70s Hughes LCLV and (b) the More Recently Fabricated Hughes LCLV.....	16
13 Response of a GEC-Marconi SLM.....	18
14 Response of the Ferroelectric Liquid Crystal SLMs.....	19
15 Experimental System used to Measure Response of LCLV with Red Read Illumination	21
16 LCLV Response as a Function of Driving Frequency	22
17 LCLV Response as a Function of Driving Amplitude.....	23
18 Experimental System Used to Measure Response of LCLV with Green Read Illumination.....	24
19 Response of Hughes LCLV to Driving Frequency for Green (514.5 nm) Write and Read Beams.....	26
20 Response of Hughes LCLV to Driving Amplitude for Green (514.5 nm) Write and Read Beams.....	27

LIST OF FIGURES (cont'd)

<u>Figure</u>	<u>Page</u>
21 Experimental System Used to Measure Response of GEC-Marconi SLM with Red Read Illumination	28
22 Response of GEC-Marconi SLM to Driving Amplitude with Optimization of Visibility per Amplitude.....	30
23 Response of GEC-Marconi SLM to Driving Frequency with Optimization of Visibility per Frequency	31
24 Response of GEC-Marconi SLM to Order of Write Light Intensity Addressing	32
25 Response of Photodetectors with Respect to Each Other	33
26 Response of GEC-Marconi SLM to Driving Frequency with optimization of visibility at 1.1 KHz	34
27 Response of GEC-Marconi SLM to driving amplitude with Optimization of Visibility at 3.1 V.....	35
28 Experimental System Used to Measure Response of FLC SLM with Red Read Illumination	36
29 FLC SLM Response at Optimal Driving Waveform.....	38
30 FLC SLM Response as a Function of Voltage.....	39
31 Binary Phase Operation FLC SLM Response.....	40
32 Equivalent Circuits for (a) Ideal Light Valve Without Write Light Illumination, (b) Ideal Light Valve with Write Light Illumination, and (c) Equivalent Circuit Voltage and Current Waveforms of an Idealized Light Valve	42
33 Circuit Model for Hughes LCLV	43
34 Typical I-V Characteristic Curve for Diodes	44
35 Circuit Model of an FLC SLM.....	47
36 I-V Characteristics for a-Si:H Photodiodes: ■: 2 μm a-Si:H; ▲: 4 μm a-Si:H.(a) Under 1 mW/cm^2 Red-light Illumination, and (b) in the Dark.....	49

LIST OF FIGURES (cont'd)

<u>Figure</u>		<u>Page</u>
37	Surface Stabilized Ferroelectric Liquid Crystal (SSFLC) Cell Geometry.....	50
38	SSFLC Read Light Modulation as a Function of Write Light Intensity for Different Temperatures.....	50
39	Joint Transform Correlator Architecture.....	52
40	Input-output Characteristic Curve of Hughes LCLV from University of Connecticut	53

I. INTRODUCTION

Optical pattern recognition systems have been proposed for use in a wide variety of applications - from systems to high-speed computing [1-3]. A major component of these systems is the Spatial Light Modulator (SLM). An SLM is a device that yields an image encoded in light from either a light or electrical signal input. SLMs have been proposed for use in the input and filter planes of coherent optical correlators [4]. An SLM in the input plane provides image conversion from an incoherent light input to an image suitable for coherent optical processing. The SLM in the filter plane acts as a programmable filter which can be dynamically cycled through a bank of filters for object identification.

The performance limitations of SLMs have significantly hampered the application of optical pattern recognition systems such as optical correlators to "real-world" problems. Liquid crystal SLMs have been constructed since the early 1970s [5]. However, these modulators have not been utilized in "real-world" environments until the late 1980s [6]. The slow response, low resolution, and high cost of spatial light modulators are currently significant limitations to "real world" application of optical pattern recognition systems that employ SLM technology. The current state-of-the-art SLMs include optically addressed nematic liquid crystal SLMs from Hughes and GEC-Marconi as well as optically addressed ferroelectric liquid crystal SLMs from Displaytech, STC Technology, and the University of Colorado-Boulder.

Preliminary experimental research has shown that the modulated read beam from some, if not all, optically addressed spatial light modulators is not linearly dependent on the write light intensity. This preliminary research was performed with a Hughes Liquid Crystal Light Valve (LCLV) and a University of Colorado-Boulder ferroelectric liquid crystal SLM [7]. Exploration of the use of nonlinear transformation in the Fourier plane of optical processors such as correlators has recently begun. Computer simulation of these nonlinear transformations on optical processors has been extensively reported [8-11]. However, the nonlinear response of optically addressed SLMs proposed for use in such nonlinear transformation processes has not been characterized. This characterization as a function of write light intensity will be presented in this report. The response will be determined for several optically addressed SLMs including Hughes LCLV, GEC-Marconi SLM, and optically addressed ferroelectric liquid crystal SLMs from University of Colorado-Boulder. The response will be reported for the candidate SLMs with respect to variations in the driving waveform frequency and amplitude, incident read beam intensity, and spectral variations in the read beam.

Section II provides a background of the basic operating principles of optically addressed liquid crystal SLMs. Section III provides a background of the state of performance of the candidate SLMs. Performance parameters discussed in this section include maximum imaging resolution, visibility or contrast ratio, and response time. Cost of these SLMs will also be discussed. Sections IV through VI outline the results of experiments performed to determine the nonlinear response of the modulated read beam as a function of write light intensity for various driving waveform frequencies and amplitudes, incident read beam intensities, and spectral variations of the write beam of the three candidate SLMs - Hughes LCLV, GEC-Marconi SLM, and optically addressed ferroelectric liquid crystal SLMs. Section VII presents the analysis and assessment of similarities, if any, of this data with respect to device construction. Section VIII discusses the effects of these nonlinearities on the performance of optical pattern recognition systems, and concludes the results of this investigation.

II. PRINCIPLES OF SPATIAL LIGHT MODULATOR (SLM) OPERATION

The function of a spatial light modulator is to modulate light in two dimensions. This is a key to exploiting the parallel processing potential of light - overcoming the limitations of the von Neumann architectures of today's computers. SLMs have been commercially available since the mid 1970s; however, performance improvements and cost reductions are still needed. While good one-dimensional modulators in the form of acousto-optic devices have been available for many years, they do not take advantage of the two-dimensional nature of optical wavefronts. Two-dimensional spatial light modulators serve this function.

For optical data processing, spatial light modulators must be capable of spatially modulating a collimated coherent beam of light in accordance with the input data to be processed. The SLM should be reusable and provide real-time operation among other properties. A wide variety of potential SLM materials and devices exist. All are in various stages of development, intended for diverse applications, and often require different optical configurations for their implementation. The technology of SLMs includes deformable mirrors [12], microchannel plates [13], magneto-optics [14], and various liquid crystal materials [15-17]. The technology related to optically addressed liquid crystal spatial light modulators will be the focus of this investigation. The basic principles of operation of these devices will be discussed in this section. Specifically, the operation of the Hughes Liquid Crystal Light Valve (LCLV), the GEC-Marconi Research's liquid crystal SLM, and the optically addressed ferroelectric liquid crystal SLMs will be discussed.

A. Liquid Crystal Light Valve (LCLV)

The basic construction of Hughes LCLV is shown in Figure 1. The LCLV has an image, usually incoherent, impressed upon the write side of the device. A coherent light source, such as a laser, is used to illuminate the incident read side of the device. The light reflected from the read side of the dielectric mirror represents a coherent image of the subject impressed on the write side of the SLM.

This device is composed of a Cadmium Sulfide (CdS) photoconductive surface followed by a Cadmium Telluride (CdTe) light absorbing layer on the input side, commonly referred to as the write side, of the device. A dielectric mirror is positioned directly against the CdTe layer. The nematic liquid crystal layer is then placed toward the read side of the device between two inert insulating layers of glass. The above assembly, from the CdS photoconductor to the inert insulating layer on the read side of the device, is then sandwiched between two transparent electrode surfaces deposited on optically flat glass. Typical operation of the LCLV requires the application of a low ac voltage, on the order of 5-10 volts, at about 1-5 KHz frequency across the electrodes. The combination of the CdS and CdTe layers creates a junction diode. The dielectric mirror thus serves two useful purposes. The mirror combined with the CdTe light absorbing layer separates the photoconductor from the read light, thereby allowing for the simultaneous writing and reading of the device. Furthermore, the reflectivity of the device can be maximized by coating the mirror for any portion of the visible spectrum desired.

The most fundamental component of the LCLV is the liquid crystal layer. The liquid crystal layer is approximately two microns thick and is operated in what is commonly referred to as a hybrid field effect mode [18]. The hybrid field effect mode utilizes conventional twisted nematic electro-optic effect in the off-state (i.e., when no voltage is applied) and optical birefringence effect for the on-state of the liquid crystal. The implementation of the hybrid field effect mode requires the construction of the liquid crystal layer such that the liquid crystal molecules are preferentially aligned with the electrode surfaces. The preferentially twisted alignment is obtained by orienting the electrode surfaces so the direction of liquid crystal alignment on the two surfaces is at some angle, 45 degrees for Hughes LCLV, with respect to each other. The twisted alignment causes the

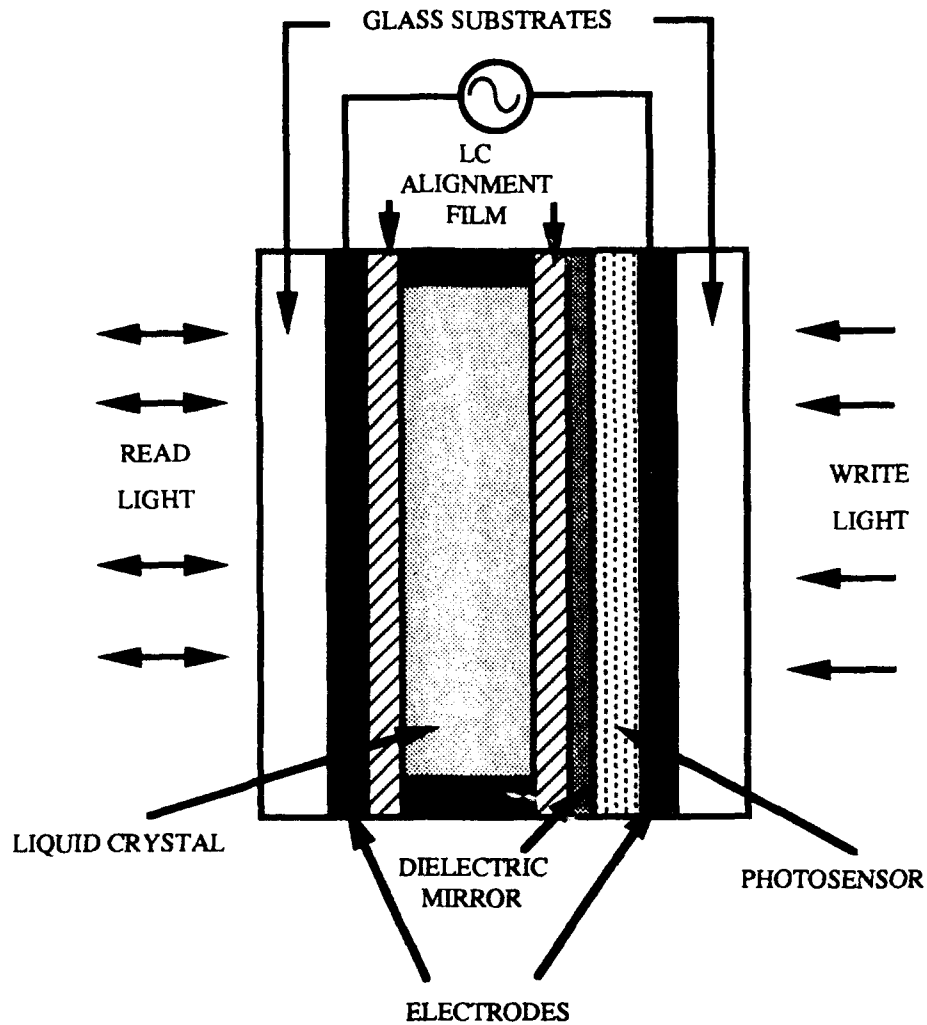


Figure 1. Schematic of Hughes LCLV

polarization of the incident light to rotate by an angle equivalent to the twist angle. An analyzer is then used in the reflected read beam of the device to provide an amplitude- or phase-modulated image of the incident write image. The Hughes LCLV ideally behaves as a $\lambda/2$ retarder of the incident read beam polarization for bright write light illuminations. Therefore, the light incident on the dielectric mirror, after a single pass through the liquid crystal layer, is retarded by $\lambda/4$ with respect to the incident linearly polarized light on the read surface. This $\lambda/4$ retardation results in the read beam being circularly polarized at the dielectric mirror/liquid crystal interface.

The interaction of the photoconductor and liquid crystal can best be understood by consideration of the simple equivalent circuit shown in Figure 2. The CdS photoconductor, CdTe light blocking layer, and twisted nematic liquid crystal are in series between the two electrode surfaces. The impedance of the CdTe and liquid crystal layers, represented as the $R_{lc}-C_{lc}$ circuit in Figure 2, is effectively constant at a particular driving frequency. A change in the impedance of the photoconductor, represented as the parallel R_s-C_s circuit in Figure 2, due to changes in incident write light irradiation, changes the voltage split between the CdS photoconductor and the CdTe/liquid crystal combination. The ac voltage across the two electrode surfaces is held constant,

so the change in impedance of the CdS is reflected in a change of voltage across the liquid crystal. The change in voltage across the liquid crystal results in a reorientation of the molecules as discussed below. C_m in Figure 2 represents the dielectric mirror.

The operation of the LCLV can be understood if a crossed polarizer/analyzer pair is placed between the LCLV and the source of the read light such that the polarizer is in the incident read beam and the analyzer is in the reflected read beam (see Figure 3). Linearly polarized light which is incident on the LCLV will be twisted by a 45 degree angle on its first pass through the liquid crystal layer. The light will then be twisted in the opposite direction by 45 degrees upon returning through the liquid crystal layer after reflection of the dielectric mirror. Therefore, the exiting light will be in phase with the incident light which would be blocked by the crossed analyzer. This dark field off-state of the device is logically explained by the twisted nematic effect. Care is exercised so that experimentally the polarization of the incident light entering the read side of the SLM is aligned along the preferential direction of the electrode surfaces in order for the twisted nematic off-state to work properly.

The polarization of the light can also remain unchanged by the application of a voltage across the electrodes which rotates the liquid crystal molecules such that the long axis of the molecules is oriented perpendicularly to the electrode surfaces. This condition would result in a dark on-state but would be of little value. However, this analogy is important to understand that an applied voltage between the full "on" and full "off" state exists such that the LCLV will transmit light through the analyzer. The liquid crystal molecules affect the polarization of the read light through optical birefringence when the orientation of these molecules is between a horizontal and perpendicular alignment of the electrodes. This occurs for some intermediate voltage between the full "on" and full "off" states.

The Hughes LCLVs utilized during this investigation were composed of CdS photoconductive surface, CdTe light blocking layer, a dielectric mirror, and twisted nematic liquid crystal. The dielectric mirror was coated for optimum use of the LCLV with a red (632.8 nm) read beam and a green (514.5 nm) write beam. The effective aperture of the LCLV was a 2- by 2 inch square with a manufacturer reported surface flatness of $< \lambda/10$.

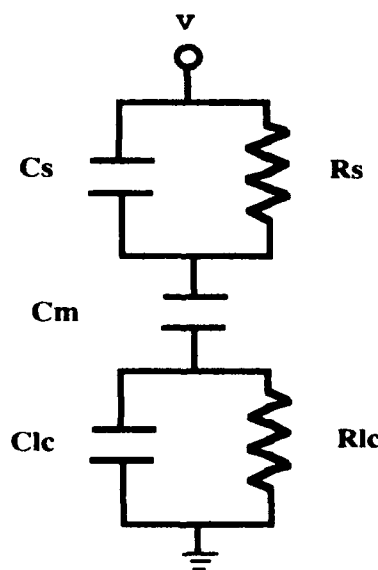


Figure 2. Elementary Circuit Model of an SLM

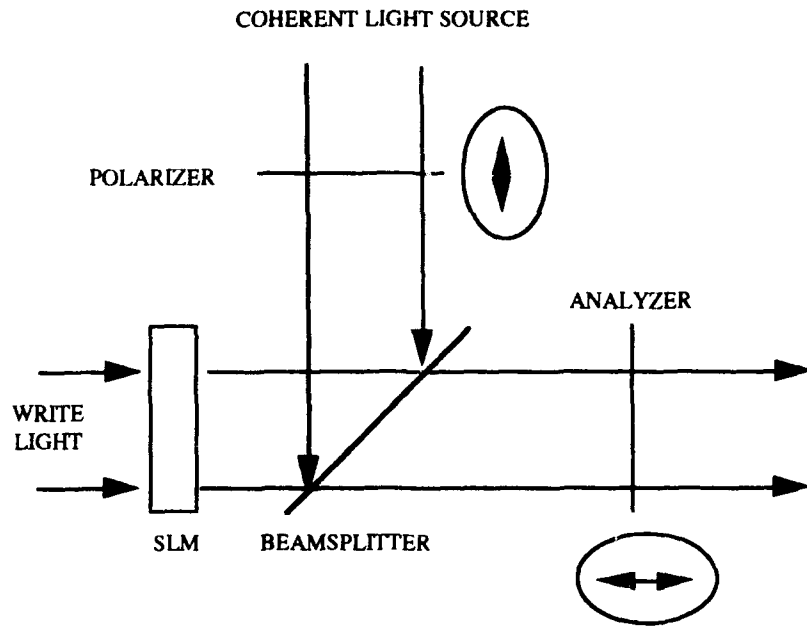


Figure 3. LCLV Operation with Polarizer/Analyzer Pair

B. GEC-Marconi Research SLM

The GEC-Marconi Research SLM is based on a sandwich structure similar to the Hughes LCLV discussed above. The key difference is the material used as the photoconductive surface. The cadmium sulfide layer of the LCLV allows for reasonable resolution but is slow responding. Crystalline silicon, used in more recent Hughes LCLVs, is fast-acting with good input light sensitivity but normally has low spatial resolution due to the thickness required [19]. The use of amorphous silicon provides high resolution while maintaining the speed and sensitivity of crystalline silicon. Care is exercised in the design of such devices to keep all layers as thin as possible to reduce any charge spreading effects that reduce resolution capabilities.

The GEC-Marconi Research SLM utilized in this investigation had a dielectric mirror coated for optimum operation of the device with green (514.5 nm) read and write beams. The effective aperture of the SLM was 40 mm by 40 mm square. The manufacturer reported surface flatness was $3\lambda/2$ over the central 3 cm surface area.

C. Optically Addressed Ferroelectric Liquid Crystal SLM

The ferroelectric liquid crystal has in recent years been considered as a candidate for optical computing or optical pattern recognition [20]. The electro-optical modulation of the material occurs when voltages of opposite signs are applied to two transparent conducting oxide layers which sandwich a slab of Ferroelectric Liquid Crystal (FLC). The voltages selected will determine the optical axis orientation which can theoretically assume one of only two possible forms, both of which are parallel to the electrode-coated optical flats and differ by an angle equivalent to twice the tilt angle of the ferroelectric material. These two orientations allow for binary operation of the cell structure. The tilt angle of most ferroelectric liquid crystal materials is 22.5 degrees over a wide

range of temperatures. Therefore, the optical axis is electrically rotated by an angle of 45 degrees per pass through the cell [21].

Figure 4 illustrates the electro-optical modulation of a transmissive ferroelectric liquid crystal element. The polarization of the FLC is chosen so the incident light is either parallel or perpendicular to one of the voltage-selected optical axis orientations so the light will be transmitted through the cell unaffected. However, if the voltage state is changed to a voltage of equal magnitude but opposite polarity, then the optical axis is rotated by 45 degrees from the incident polarization. The thickness of the FLC material is chosen so a total phase shift of π will occur for light passing through the cell under this condition. Therefore, the incident light's polarization will be rotated by 90 degrees for a dark field effect. Typical voltages used for the modulation of FLC are small --- on the order of +/- 16 V.

Optically addressed ferroelectric liquid crystal SLMs have been fabricated by the University of Colorado-Boulder, Displaytech, and STC Technologies. The FLC SLMs utilized during this investigation were fabricated by the University of Colorado-Boulder and Displaytech. The basic construction and theory of operation of these SLMs is similar to the Hughes LCLV and the GEC-Marconi Research SLM. Amorphous silicon is used as the photosensor and the liquid

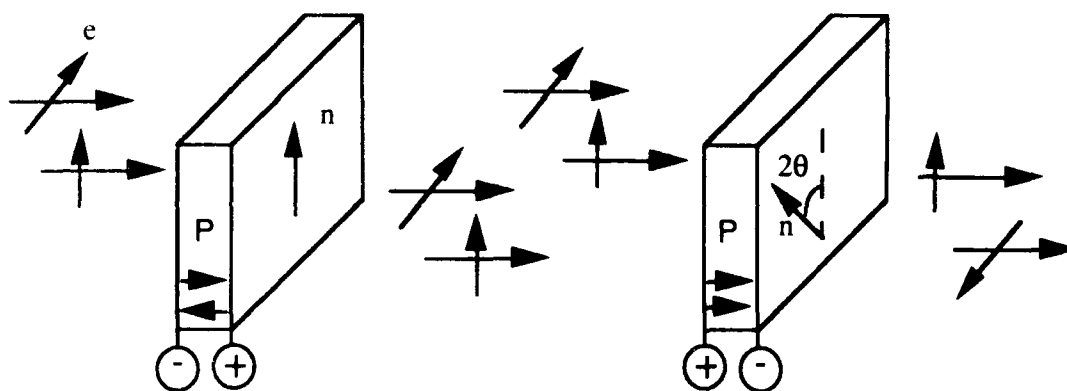


Figure 4. Electro-optical Modulation of FLC

crystal is ferroelectric in nature. The ferroelectric liquid crystal is Smectic C*. Typical operation of the FLC devices requires the application of a 17 V peak-to-peak amplitude of a 1 KHz square wave with a small DC offset voltage (typically +2 V).

Three FLC SLMs were available for this investigation. Two were jointly produced by the University of Colorado-Boulder and Displaytech. These two devices are the first known optically addressed SLMs that used ferroelectric liquid crystals as the modulating medium. Because of their prototype evolutionary state, these devices did not employ optical flats to sandwich the structure or a dielectric mirror. The absence of the dielectric coatings allowed for the unwanted transmission of the write beam through the liquid crystal. A great deal of unmodulated light was transmitted by these devices when they were addressed with a broadband white light. Experimentally, it was found that green light was well absorbed while still providing enough activation energy for the amorphous silicon photosensor. The absence of the dielectric mirrors also resulted in cautious operation of the SLM to prevent the read light from being of a sufficient

intensity to enter the photosensor and write a DC bias term. Without the dielectric mirror present, the reflectivity of the device is determined by the step in the refractive index at the amorphous silicon/liquid crystal interface. This refractive index difference resulted in a reflectivity of approximately 20 percent of the read beam. Furthermore, the glass plates, as opposed to optical flats, in these modulators created an interference pattern of Newton rings in the modulated read image. These rings increased the average of the background noise of the modulated image and thus decreased the visibility (or contrast ratio) available from these SLMs.

The third FLC SLM was manufactured by Displaytech. This device utilized optical flats and a dielectric mirror. The mirror was coated for optimum use of the SLM with a green (514.5 nm) write beam and a red (632.8 nm) read beam. The optical flats and dielectric mirrors erased the problems associated with the two modulators discussed above.

III. SLM PERFORMANCE CHARACTERISTICS

The performance characteristics of three unique optically addressed SLMs have been experimentally investigated. The measured parameters include maximum resolution, visibility, imaging response time, and write light sensitivity. The modulators investigated include two relatively new technologies, the FLC SLM from the University of Colorado-Boulder and the amorphous silicon photoconductive twisted nematic liquid crystal SLM from GEC-Marconi Research, and a well established industry benchmark, the Hughes LCLV.

This section is a compilation of operating parameters and performance of the above modulators. The parameters investigated aid in understanding the utility of these modulators as input image transducers, specifically in optical correlator architectures. The resolution, visibility, and response time of each modulator was measured and the results are presented here for comparison.

A. Resolution Measurements

The experimental system shown in Figure 5 was used to measure the resolution of the candidate SLMs. A HeNe laser ($\lambda=632.8$ nm) was spatially filtered and collimated using standard laboratory techniques. A polarizing beamsplitter was used to direct the HeNe beam to the read side of the SLM. Lenses L2 and L3 were used to image the modulated read beam onto a CCD camera. The position and focal length of lenses L2 and L3 were chosen to provide a 4:1 magnification of the modulated read beam. The input polarizer and polarizing beamsplitter were also oriented for optimum image visibility at the CCD plane. An argon ion laser was employed as the write light source. The argon laser was also spatially filtered and collimated using standard laboratory techniques. The collimated argon beam ($\lambda=514.5$ nm) was incident on a chrome-on-glass transparency of a USAF Resolution Chart. The illuminated chart was then imaged onto the write side of the SLM using lens L1, a 50 mm focal length compound lens assembly. The focal length and position of the lens was chosen for unity magnification of the chart onto the SLM write surface. Initially, no SLM was present in the test system in order to measure the maximum resolution of the imaging optics. A photograph of the resultant image is shown in Figure 6. The smallest resolvable segment of the USAF resolution chart was found in group #6, element #5 which corresponds to a maximum resolution of 102 lp/mm.

A Hughes LCLV was initially tested with the above system. The Hughes LCLV employs CdS as the photoconductor and a twisted nematic liquid crystal structure as the active modulating medium. Maximum resolution was achieved when this device was driven by a 1.92 KHz, 9.96 V amplitude sinusoidal waveform while the incident read and write beam intensities corresponded to $140 \mu\text{W}/\text{cm}^2$ each. A photograph of the modulated read beam image is shown in

Figure 7(a). The maximum resolution was found in group #5, element #3 which corresponds to 40 lp/mm. This particular LCLV was fabricated in the late 70s. This modulator was replaced in the optical testbed with a more recently fabricated LCLV, also manufactured by Hughes. This more recent LCLV also employed CdS and a twisted nematic liquid crystal structure. The intensities of the write and read beams were measured to be 100 and 80 $\mu\text{W}/\text{cm}^2$, respectively. The driving waveform and read beam polarization were adjusted until maximum resolution was observed at the CCD plane. Maximum resolution was determined to be 22.6 lp/mm (group # 4,

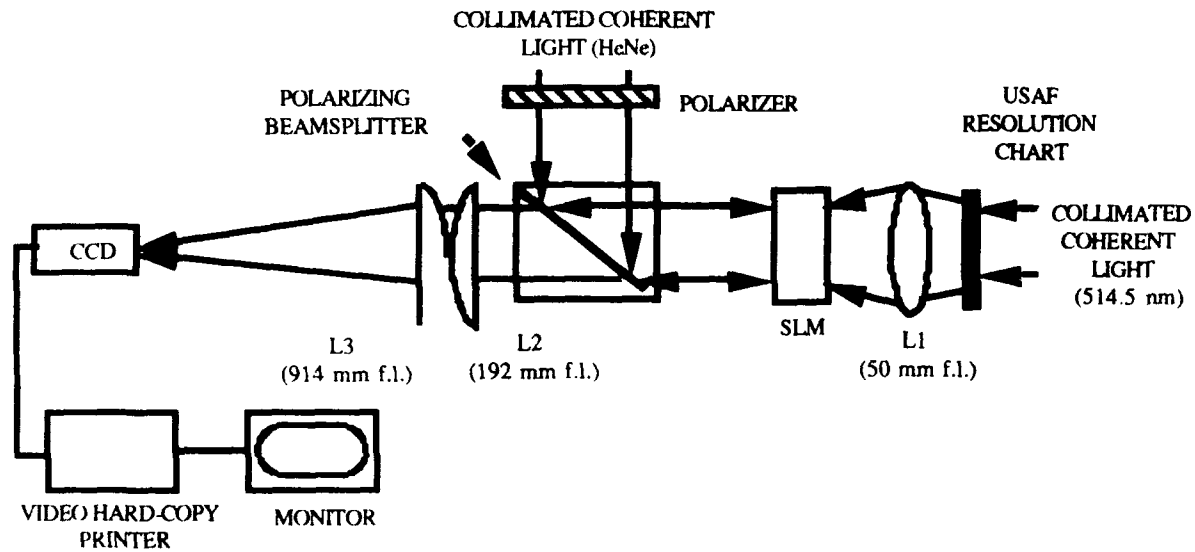


Figure 5. SLM Resolution Measurement System

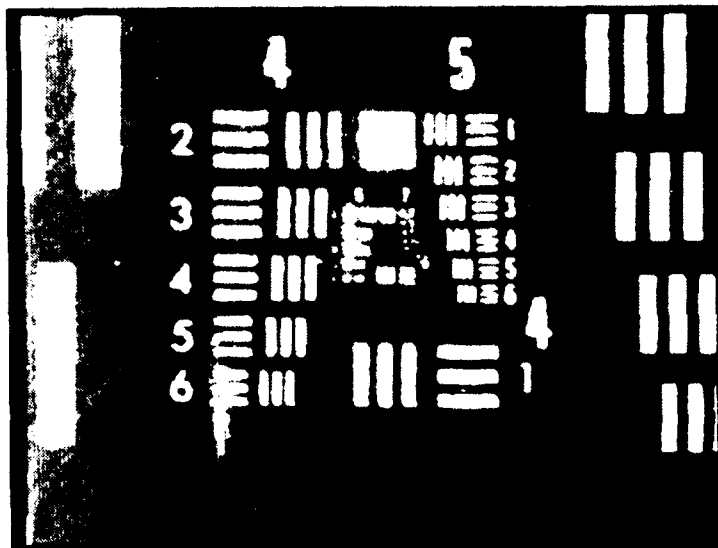
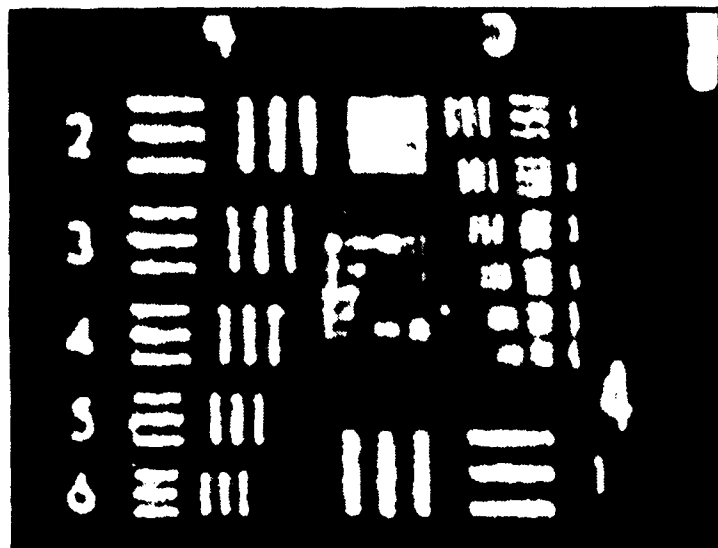
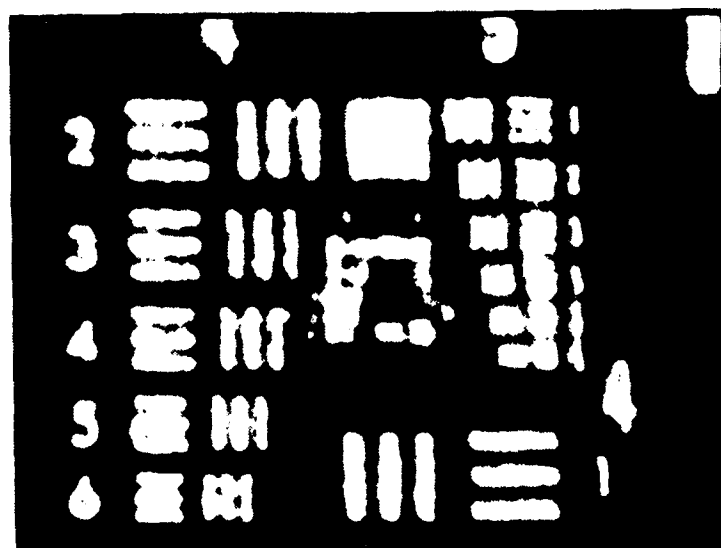


Figure 6. Resolution Limit of System Shown in Figure 5

element #4) as shown by the photograph in Figure 7(b). The driving waveform corresponding to this maximum resolution condition was a 4 KHz, 7.97 V sinusoid. The difference in resolution between the Hughes LCLVs may be attributed to variations that occurred in the manufacture of the LCLVs, specifically, the alignment process of the multilayer sandwich structures.



(a)



(b)

Figure 7. Resolution of the Hughes LCLVs

The Hughes LCLVs were then replaced with an optically addressed SLM available from GEC-Marconi Research. This SLM utilizes hydrogenated amorphous silicon as the photoconductor and a twisted nematic liquid crystal structure as the modulating medium. Again, the driving waveform and read beam polarization were adjusted until maximum resolution was observed at the CCD plane. Initially, the write light incident on the SLM corresponded to $600 \mu\text{W}/\text{cm}^2$. Maximum resolution was determined to be 71.8 lp/mm while the driving waveform of the SLM was a 5 KHz, 3.5 V sine wave. Alternatively, maximum resolution was determined to be 64 lp/mm (group #6, element #1) for lower write light intensities ($100 \mu\text{W}/\text{cm}^2$). This resolution measurement for low write light intensities occurred when the GEC-Marconi SLM was driven by a 1.5 KHz, 2 V square wave with a +1 V DC offset. A photograph of the corresponding image is shown in Figure 8.

The GEC-Marconi SLM was then replaced by an optically addressed FLC SLM fabricated by the University of Colorado-Boulder and Displaytech, Inc. The basic structure of this modulator was discussed in Section II. Optimum resolution was observed when the incident write beam intensity corresponded to $300\text{-}500 \mu\text{W}/\text{cm}^2$. Maximum resolution was determined to be 71.8 lp/mm when the incident write light intensity corresponded to $300 \mu\text{W}/\text{cm}^2$. For optical correlation applications, lower write light intensities are usually required. The write beam was attenuated with a variable beamsplitter until $100 \mu\text{W}/\text{cm}^2$ was incident on the FLC SLM write surface. The driving waveform and read beam polarization were adjusted until maximum resolution and image visibility occurred. The optimum resolution and visibility were both very low. The sensitivity of the device to input scenes corresponding to the above stated intensity was immeasurable. The write beam intensity was then increased to $200 \mu\text{W}/\text{cm}^2$ incident on the FLC SLM. This intensity was a compromise between the write light intensity required to achieve

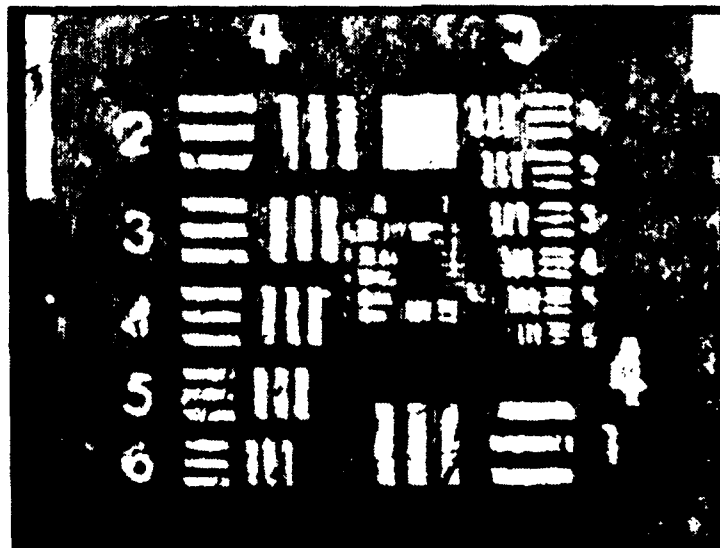


Figure 8. Resolution of the GEC-Marconi Research SLM

maximum resolution and the intensity commonly needed in optical correlator architectures. Maximum resolution was determined to be 64 lp/mm at 200 $\mu\text{W}/\text{cm}^2$ incident write light while the driving waveform was a 1.25 KHz, 15 V square wave with a +5 V DC offset. A photograph of the resultant image is shown in Figure 9(a).

A second FLC SLM was tested in the system depicted in Figure 5. This FLC SLM was also fabricated by the University of Colorado-Boulder and Displaytech, Inc. At 500 $\mu\text{W}/\text{cm}^2$ incident write beam intensity, maximum resolution was determined to be 102 lp/mm while the driving waveform was a 1 KHz, 9 V square wave with a +3 V DC offset. This resolution measurement corresponds to the maximum resolution of the imaging optics of the testbed. The source of the resolution limit of the experimental system is believed to be twofold. First, the lenses used within the system are believed to be MTF limited at approximately 100 lp/mm. Secondly, the magnification chosen for the imaging optics extended the useful resolving power of the CCD camera from 25-30 lp/mm to 100 lp/mm by choosing the position and focal length of the read beam imaging lens to achieve an image magnification of 4:1. Therefore, the maximum resolution of the FLC SLM may well be greater than 100 lp/mm for a 500 $\mu\text{W}/\text{cm}^2$ incident write light intensity. Again, the write beam was attenuated with a variable beamsplitter until the incident light on the write surface of the SLM corresponded to 200 $\mu\text{W}/\text{cm}^2$. The maximum resolution was determined to be 71.8 lp/mm (group #6, element #2) for this condition. The driving waveform of the device was a 1 KHz, 10 V square wave with a +5 V DC offset. A photograph of the resultant image is shown in Figure 9(b).

The above resolution measurements are summarized in Table 3.1 along with the resolution corresponding to 50% visibility discussed in the following section.

B. Visibility Measurements

The experimental system shown in Figure 10 was used to measure the visibility of the candidate SLMs. The system shown in Figure 10 differs from the one shown in Figure 5 by the addition of a Colorado Video model 321 video analyzer and a strip-chart recorder. The output video of the CCD camera was channeled to the video analyzer. The analyzer was then used to perform a horizontal or vertical scan across each group and element of the USAF resolution image. The relative intensity of the scans was recorded via an OmniScribe D5000 series chart recorder. Following Michelson [22], visibility is defined as:

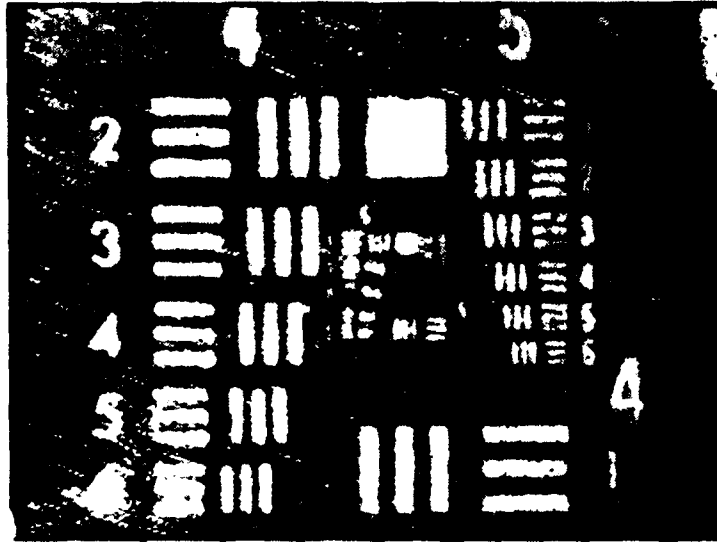
$$v = \frac{I_{\max} - I_{\min}}{I_{\max} + I_{\min}} \quad (1)$$

where I_{\max} and I_{\min} are the maximum and minimum intensities of the resulting image. The visibility of each group and element number was determined using the above technique. The group and element number of the USAF resolution image corresponding to a visibility of 0.50 for each SLM was particularly noted.

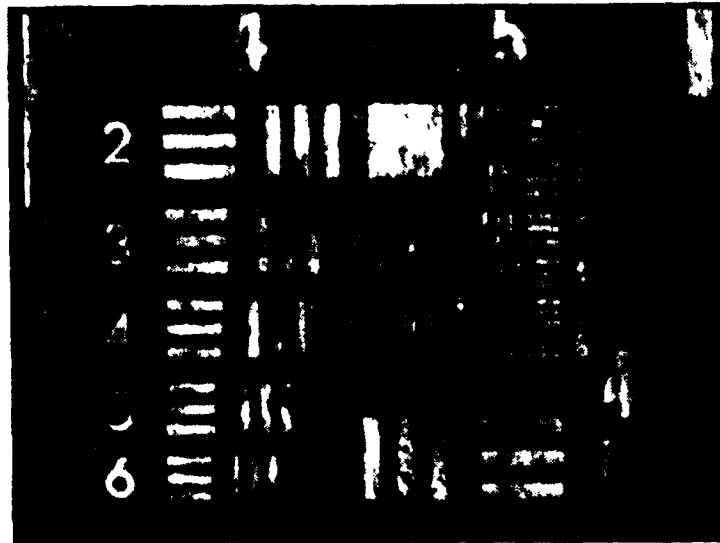
The resolution corresponding to 50 percent visibility for each of the above modulators was determined using the same conditions of operation (write light intensity and driving waveform) for each of the modulators described above. A summary of these measurements is shown in Table 1.

Table 1. Tabulated SLM Resolution and Visibility Data

SLM	MAX RESOLUTION	RESOLUTION@0.50	WRITE INTENSITY
HUGHES LCLV	40 lp/mm	20 lp/mm	140 μ W/sq.cm.
PCU SLM (Hughes LCLV)	22 lp/mm	18 lp/mm	100 μ W/sq.cm.
GEC-Marconi SLM	64 lp/mm	32 lp/mm	100 μ W/sq.cm.
FLC #1 SLM	64 lp/mm	40 lp/mm	200 μ W/sq.cm.
FLC #2 SLM	71.8 lp/mm >102 lp/mm	20 lp/mm -----	200 μ W/sq.cm. 500 μ W/sq.cm.



(a)



(b)

Figure 9. Resolution of the Ferroelectric Liquid Crystal SLMs

C. Response Time Measurements

The response times of the candidate modulators were measured using the experimental system shown in Figure 11. The inclusion of an electronic shutter in the write beam and a modification of the read beam output optics are the key differences between this testbed and the one described in Figure 5. Lenses L2 and L3 of Figure 5 were replaced with a single 254 mm focal length bi-convex lens. This lens was chosen to capture the entire modulated read beam onto a Newport Research Corp. model 815-SL power meter/photodetector assembly. The analog output of the power meter was then sampled using an A/D data acquisition board located within an IBM AT chassis. Alternatively, the output of the power meter could be viewed with an oscilloscope.

Prior to collection of data using this system, the response time limitation of the shutter, detector, and A/D acquisition was determined. The detector was positioned in front of the shutter of the write beam, which was cycled open and closed every 40 milliseconds. The A/D board sampled the output of the detector every 0.2 milliseconds during this cycling. The rise and fall times were determined to be approximately one millisecond each for the shutter/detector combination. Therefore, the detector, shutter, and A/D acquisition process should not limit the response measurement of the candidate modulators until about 500 Hz.

The Hughes LCLVs were first tested using the system described above. The shutter, and therefore the write beam incident on the modulator, was cycled "on" and "off" for each modulator. The analog output of the photodetector was sampled and the resultant plots of response time for the two Hughes LCLVs are shown in Figure 12. The write and read beams incident on the late 1970s LCLV corresponded to $100 \mu\text{W}/\text{cm}^2$ and $80 \mu\text{W}/\text{cm}^2$ intensity, respectively. Response

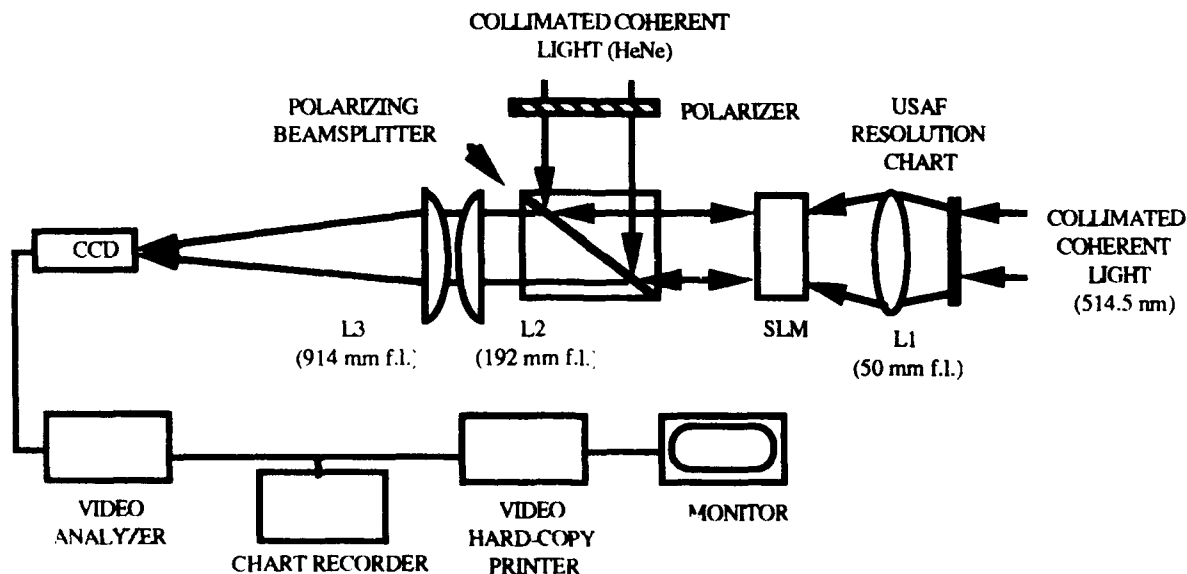


Figure 10. Visibility Measurement System

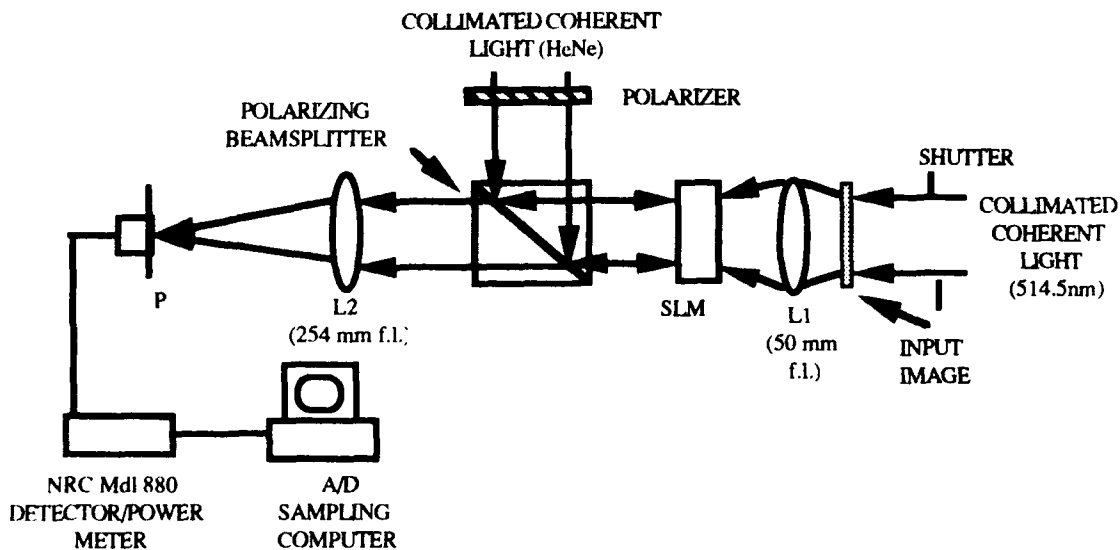
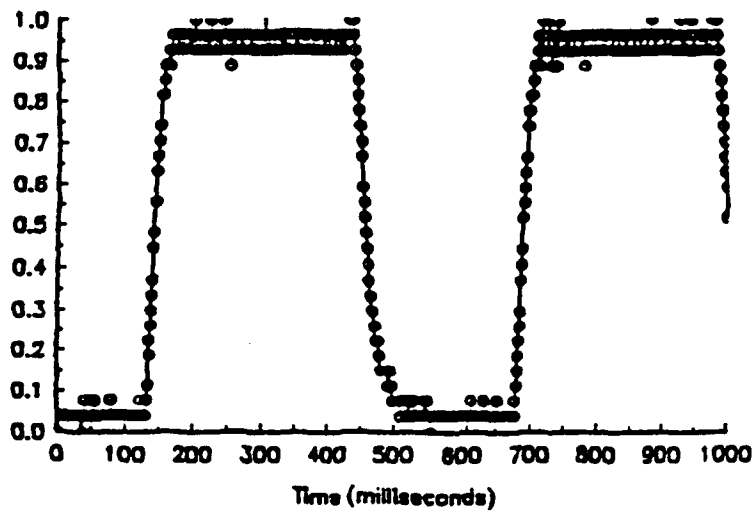


Figure 11. Response Time Measurement System

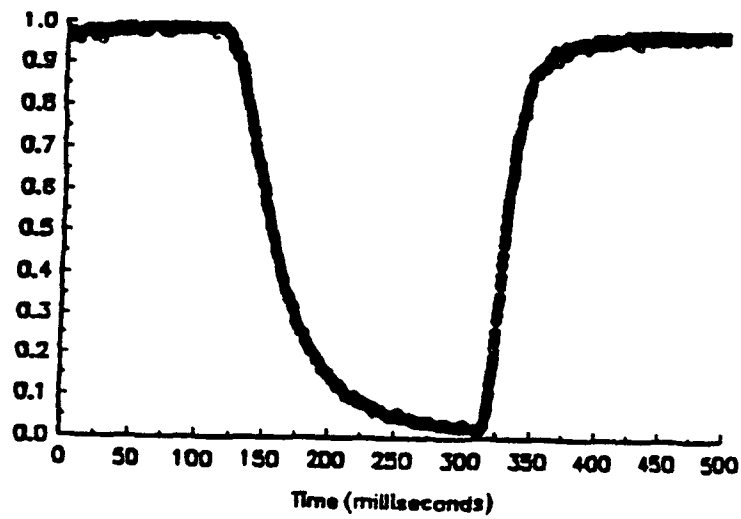
of SLMs is typically quoted as a function of two values – rise and fall times. Furthermore, the rise time is typically quoted from the 10 percent to 90 percent of full modulation whereas fall time is quoted as the 90 percent to 10 percent of full modulation. The 10-90 percent rise time was measured as 22 milliseconds whereas the 90-10 percent fall time was measured as 52 milliseconds for a total cycle time of 74 milliseconds. Alternatively, the 0-100 percent rise time was measured as 35 milliseconds, the 100-0 percent fall time was 77 milliseconds, and the total cycle time was 112 milliseconds. The response of the more recently fabricated Hughes LCLV was also measured. The response was measured with incident write and read beam intensities of 100 and 80 $\mu\text{W}/\text{cm}^2$, respectively. The 10-90% rise time was determined to be 27 milliseconds, whereas the 90-10 percent fall time was 77 milliseconds. Alternatively, the 0-100 percent rise time was 54 milliseconds and the 100-0 percent fall time was 140 milliseconds for this device.

The Hughes LCLVs were replaced with the GEC-Marconi Research SLM in the experimental system depicted in Figure 11. The resultant response curve is shown in Figure 13. The 10-90 percent rise time was measured to be 6 milliseconds while the 90-10 percent fall time was 19 milliseconds. The 0-100 percent rise time was determined to be 11 milliseconds, whereas the 100-0 percent fall time was 40 milliseconds. The write and read beam intensities corresponding to these measurements were 100 and 10 $\mu\text{W}/\text{cm}^2$, respectively.

The GEC-Marconi SLM was then replaced with the earlier version of the FLC SLM fabricated by the University of Colorado-Boulder and Displaytech, Inc. The response of this modulator was measured using the techniques described above. The resultant response curve is shown in Figure 14(a). The 10-90 percent rise time was measured to be 5 milliseconds whereas the 90-10 percent fall time was determined to be 4 milliseconds. The 0-100 percent rise time was measured to be 10 milliseconds, whereas the 100-0 percent fall time was determined to be 8 milliseconds. These response measurements occurred at 600 $\mu\text{W}/\text{cm}^2$ write light intensity and 25 $\mu\text{W}/\text{cm}^2$ read light intensity.



(a)



(b)

Figure 12. Response of (a) the Late 70s Hughes LCLV and
(b) the More Recently Fabricated Hughes LCLV

The SLM was then replaced with a more recently fabricated FLC SLM, also from the University of Colorado-Boulder and Displaytech, Inc. The electronic shutter was cycled open and closed at a 5 Hz frequency. A high frequency modulation observed on the response curve was due to the device being driven by the 1.0 KHz square wave voltage. The reason that the output of the device oscillates at this frequency is because the device at least partially erases during the forward-bias portion of the square wave cycle. Ideally, the device would completely erase during every forward bias period, but the photoconductive effects of the amorphous silicon photosensor presently limit this response. The large amplitude of this high frequency modulation obscured the rise and fall times of the optical response. Analog filtering was employed prior to the A/D sampling to more clearly determine the optical response of the modulator while suppressing the electrical response due to the driving frequency. Several low-pass filters were utilized. The cutoff frequency of these filters included 500, 200, and 100 Hz. Comparison of the resulting response curves using these varying filters revealed no characteristic change in the shape of the optical response while successfully suppressing most of the high frequency modulation. Figure 14(b) shows the optical response of the FLC modulator using a low-pass analog filter with a 100 Hz cutoff frequency. The rise time, measured from the baseline to the maximum value, was 6 milliseconds. The fall time, from maximum value to the baseline, was 8 milliseconds. The cycle time is 14 milliseconds which corresponds to approximately 70 Hz. This response was taken near the optimum visibility of the modulator with $500 \mu\text{W}/\text{cm}^2$ incident on the write side of the device. The device was driven with a 1 KHz, 10 V square wave with a +5 V DC offset. The above response time measurements are summarized in Table 2.

Table 2. Summary of Response Time Data for the Candidate SLMs

SLM	RISE TIME 10%-90% / 0%-100%	FALL TIME 10%-90% / 0%-100%	WRITE INTENSITY
HUGHES LCLV	22 msec / 35 msec	52 msec / 77 msec	100 $\mu\text{W}/\text{sq. cm.}$
PCU SLM (Hughes LCLV)	27 msec / 54 msec	77 msec / 140 msec	100 $\mu\text{W}/\text{sq. cm.}$
GEC-Marconi Research SLM	6 msec / 11 msec	19 msec / 40 msec	100 $\mu\text{W}/\text{sq. cm.}$
FLC #1 SLM	5 msec / 10 msec	4 msec / 8 msec	600 $\mu\text{W}/\text{sq. cm.}$
FLC #2 SLM	----- / 6 msec	----- / 8 msec	500 $\mu\text{W}/\text{sq. cm.}$

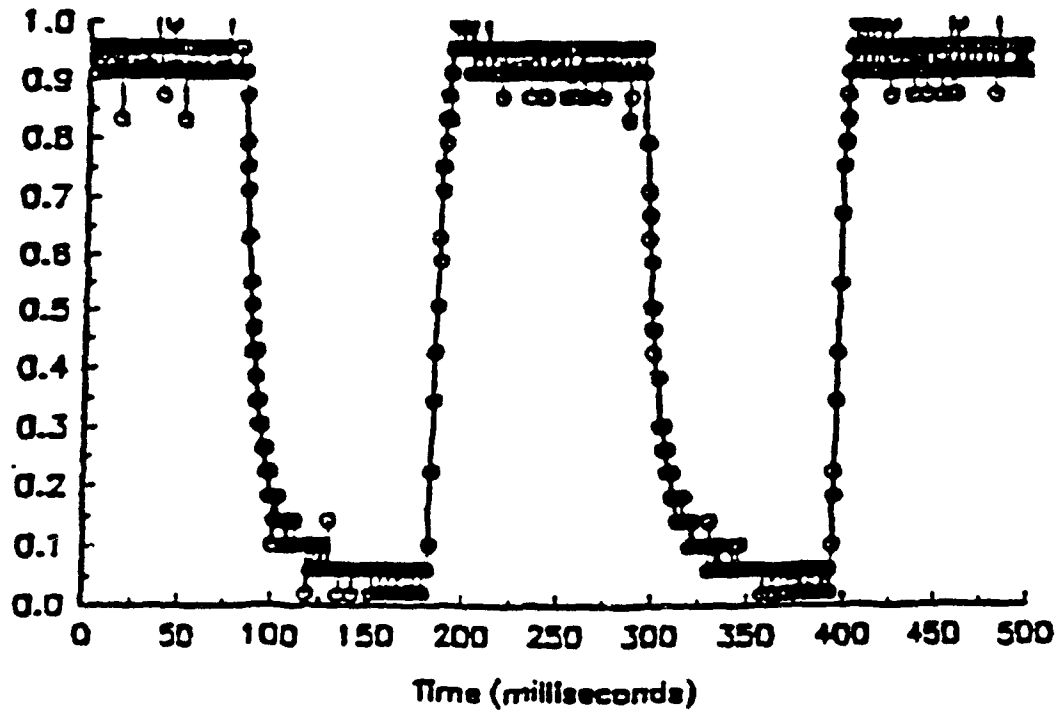
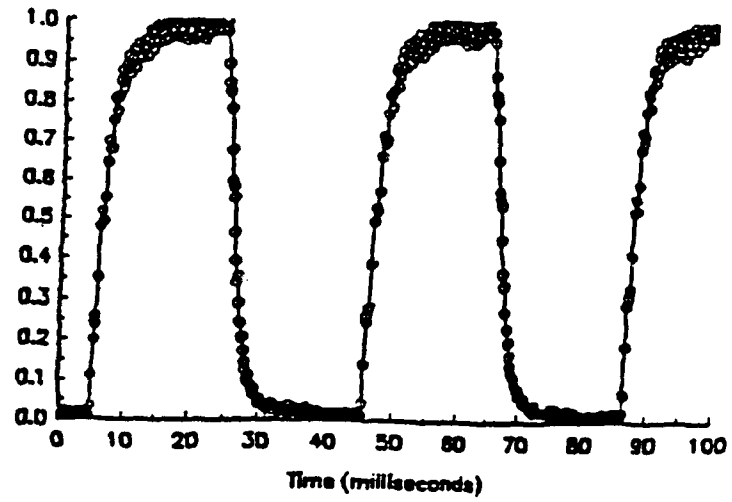
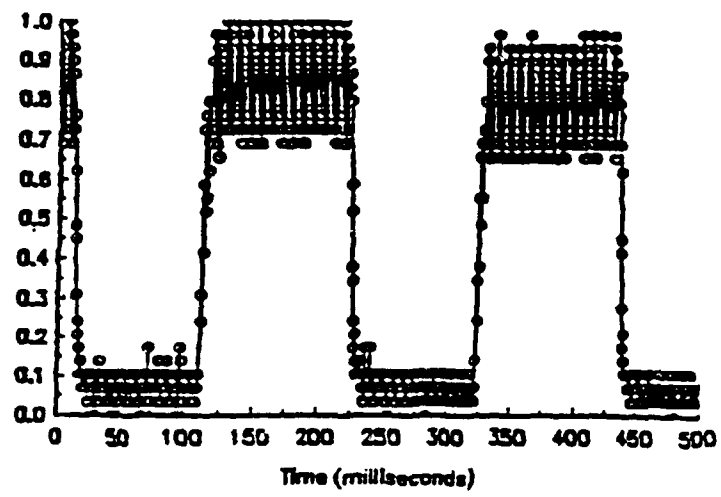


Figure 13. Response of a GEC-Marconi SLM

Key performance parameters of several optically addressed SLMs have been experimentally determined. These parametric measurements included maximum resolution, visibility, and response time of Hughes, GEC-Marconi, and FLC SLMs. The measurements are not necessarily intended to present absolute values for the performance of the candidate modulators; however, they do provide an accurate means of comparing SLMs due to the identical test techniques used.



(a)



(b)

Figure 14. Response of the Ferroelectric Liquid Crystal SLMs

IV. HUGHES LIQUID CRYSTAL LIGHT VALVE (LCLV) NONLINEAR RESPONSE

Recently, the effects of a nonlinear matched filter in optical correlator architectures have been investigated [23]. The operation of this nonlinear matched filter has been simulated for various correlator architectures. However, the nonlinear response of most SLMs typically utilized in these correlators has not been experimentally measured. The response of several SLMs has been measured and will be discussed within this report. These responses were measured for varying illuminations and driving waveform amplitudes and frequencies. The modulators tested include the Hughes CdS LCLV, the GEC-Marconi SLM, and the optically addressed FLC SLMs. Furthermore, the response was measured for varying read light spectra from red to green for the LCLV and GEC-Marconi SLM. The response of the optically addressed ferroelectric SLMs as a function of read light spectra was not measured due to the lack of a dielectric mirror to effectively isolate the read and write beams from each other for proper activation of the photosensor.

The details of the response measurement of the LCLV are discussed within this section, the GEC-Marconi SLM is discussed in Section V, and the FLC SLM in Section VI.

A. LCLV Response to 632.8 nm Read Beam Illumination

The experimental system shown in Figure 15 was used to measure the response of the Hughes LCLV as a function of write light intensity for various driving waveforms and amplitudes while maintaining a fixed spectral addressing of red ($\lambda=632.8$ nm) read beam and a green ($\lambda=514.5$ nm) write beam. A Spectra-Physics model 124B HeNe laser was spatially filtered and collimated using standard laboratory techniques. The spatial filter consisted of a 20x objective and 15 μm pinhole. The collimating lens was a bi-convex doublet with an effective focal length of 50 mm. A polarizer was then used to selectively address the read surface of the LCLV with vertically polarized light via a nonpolarizing beamsplitter. Polarizer P3 was used as an analyzer of the modulated read beam to observe an optimal amplitude modulated image at Detector #2 via lens L3. L3 was a biconvex lens with a focal length of 254 mm and Detector #2 was a Newport Research Corporation (NRC) model 818SL silicon photodetector mated to an NRC model 835 power meter. The neutral density filters in the read beam were used to attenuate the light incident on the read surface of the LCLV. The light incident on this surface was measured to be approximately 10 $\mu\text{W}/\text{cm}^2$. The write beam to the LCLV was constructed from a Spectra-Physics model 2020 argon ion laser source. This source was spatially filtered and collimated using a 20x objective, 15 μm pinhole, and a biconvex lens with a focal length of 254 mm. Polarizer P1 was used to preferentially address the write surface of the LCLV with vertically polarized light via a nonpolarizing beamsplitter. A variable beamsplitter/attenuator, VBS, was inserted in the write beam prior to the nonpolarizing beamsplitter to provide a means of varying the write light intensity incident on the write surface of the LCLV and the reference write beam photodetector D1.

Initially, a USAF resolution transparency was imaged onto the write surface of the LCLV via lens L2, a compound imaging lens with an effective focal length of 50 mm. The driving waveform, amplitude, and frequency, as well as the orientation of the analyzer P3, were varied until an image of optimal visibility was observed at detector plane D2. The silicon photodetector/power meter located in this plane was temporarily replaced with a CCD camera to observe the modulated read beam image. The optimum driving signal for the LCLV was determined to be a 1.92 KHz sinusoid with an amplitude of 9.96 volts. This image corresponded to a write light intensity of 100 $\mu\text{W}/\text{cm}^2$ incident on the SLM. The driving frequency of the Hughes LCLV was reduced to 1 KHz.

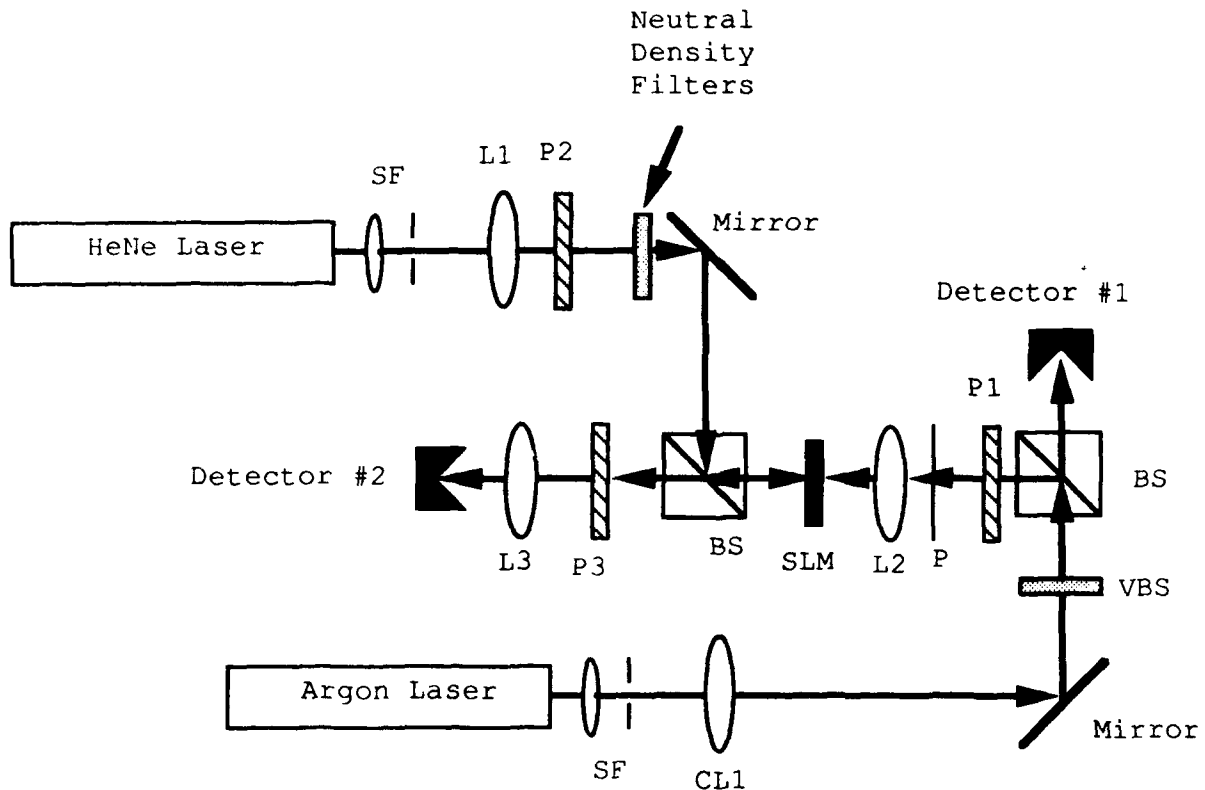


Figure 15. Experiment System Used to Measure Response of LCLV with Red Read Illumination

The silicon photodetector was repositioned at plane D2 and the variable attenuator rotated over an extended range. The read and write intensities of detector D2 and D1, respectively, were recorded as the write light incident on the LCLV was altered. The resultant response of the LCLV modulated read beam as a function of write light intensity is shown in Figure 16. Data was also taken for driving frequencies of 2 KHz and 5 KHz. In order to achieve an image of optimal visibility at D2, Analyzer P3 was not adjusted at the beginning of each data run. The resulting data is plotted with the 1 KHz frequency data in Figure 16.

The maximum intensity of the modulated read beam, shown in Figure 16, was measured to be approximately $2.5 \mu\text{W}/\text{cm}^2$ at plane D2. This value is considerably less than the $10 \mu\text{W}/\text{cm}^2$ incident on the read surface of the LCLV. More detailed analysis of the read beam intensity at various locations along its path was performed. The intensity of the reflected read beam was measured for two different operating conditions of the LCLV— without any write light illumination and with approximately $100 \mu\text{W}/\text{cm}^2$ write light incident on the LCLV. Prior to polarizer P3 but after transmission of the reflected read beam through the beamsplitter, the read beam intensity was measured to be 4.5 and $3.25 \mu\text{W}/\text{cm}^2$ for $100 \mu\text{W}/\text{cm}^2$ and zero intensity write light illuminations, respectively. Analyzer P3 was oriented for optimum amplitude modulation, i.e., visibility, of the image at plane D2. Consequently, a significant amount of read light which is

1.0 KHz case:

$$I_r = 0.774 \left\{ 1 - \exp \left(\frac{-I_w}{166} \right) \right\} + 0.0856$$

2.0 KHz case:

$$I_r = 0.724 \left\{ 1 - \exp \left(\frac{-I_w}{141} \right) \right\} + 0.144$$

5.0 KHz case:

$$I_r = 0.808 \left\{ 1 - \exp \left(\frac{-I_w}{193} \right) \right\} + 0.0588$$

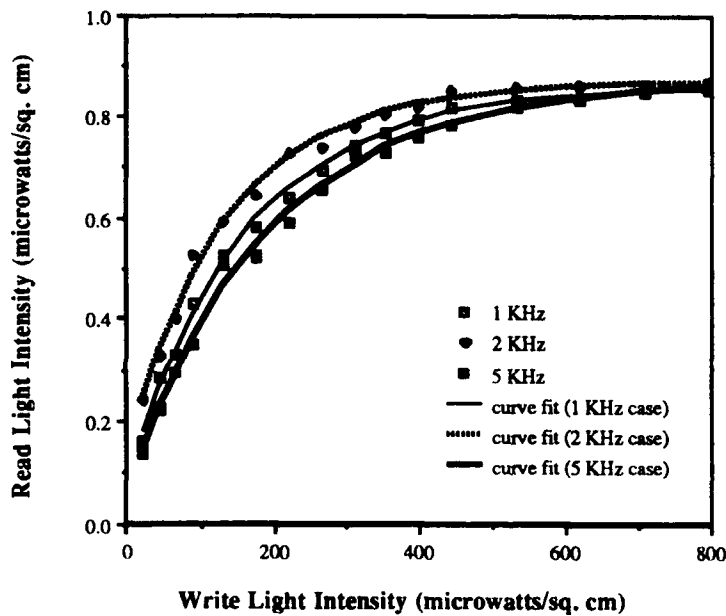


Figure 16. LCLV Response as a Function of Driving Frequency

not polarized in the same plane as the transmission axis of P3 is blocked. The modulated read beam after transmission through P3 was measured to be $1.1 \mu\text{W}/\text{cm}^2$ and $60 \text{ nW}/\text{cm}^2$ for $100 \mu\text{W}/\text{cm}^2$ and zero write light intensities, respectively.

Next, the response of the LCLV was measured as a function of the driving amplitude. Again, the read and write beam intensities were recorded as the write light incident on the LCLV was altered. Initially, the LCLV was operated with a 1.92 KHz 10 V sinusoidal driving signal. Data for driving amplitudes of 8.0, 10.0, and 12.0 V are shown graphically in Figure 17.

8.0 V case:

$$I_r = 0.923 \left\{ 1 - \exp \left(\frac{-I_w}{353} \right) \right\} - 0.0178$$

10.0 V case:

$$I_r = 0.715 \left\{ 1 - \exp \left(\frac{-I_w}{94.9} \right) \right\} + 0.167$$

12.0 V case:

$$I_r = 1.40 \left\{ 1 - \exp \left(\frac{-I_w}{12.5} \right) \right\} - 0.576$$

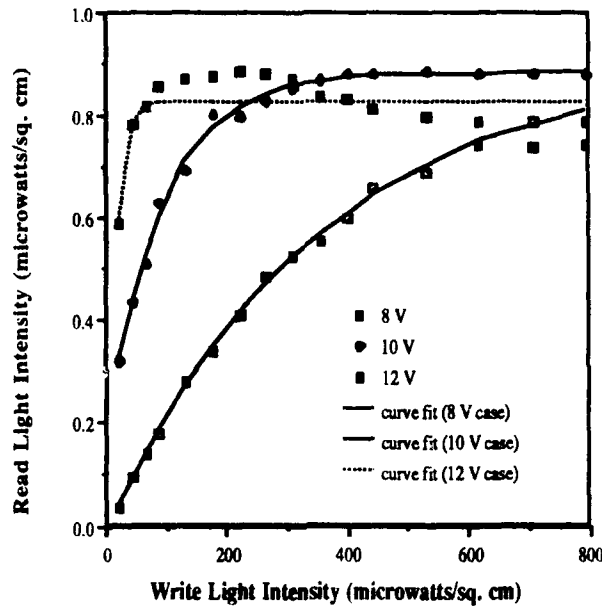


Figure 17. LCLV Response as a Function of Driving Amplitude

B. LCLV Response to 514.5 nm Read Beam Illumination

The response of the LCLV was also measured as a function of driving amplitudes and frequencies when green illumination was used for both the read and write beams. The experimental system used to measure this response is shown in Figure 18. A Spectra-Physics model 2020 argon ion laser was spatially filtered and collimated using standard laboratory techniques. The spatial filter consisted of a 20x objective and 15 μm pinhole. The collimating lens had a focal length of 189 mm. The collimated beam was divided into two equal intensity beams by beamsplitter BS1. The reflected and transmitted beams were directed to the write and read surfaces of the LCLV.

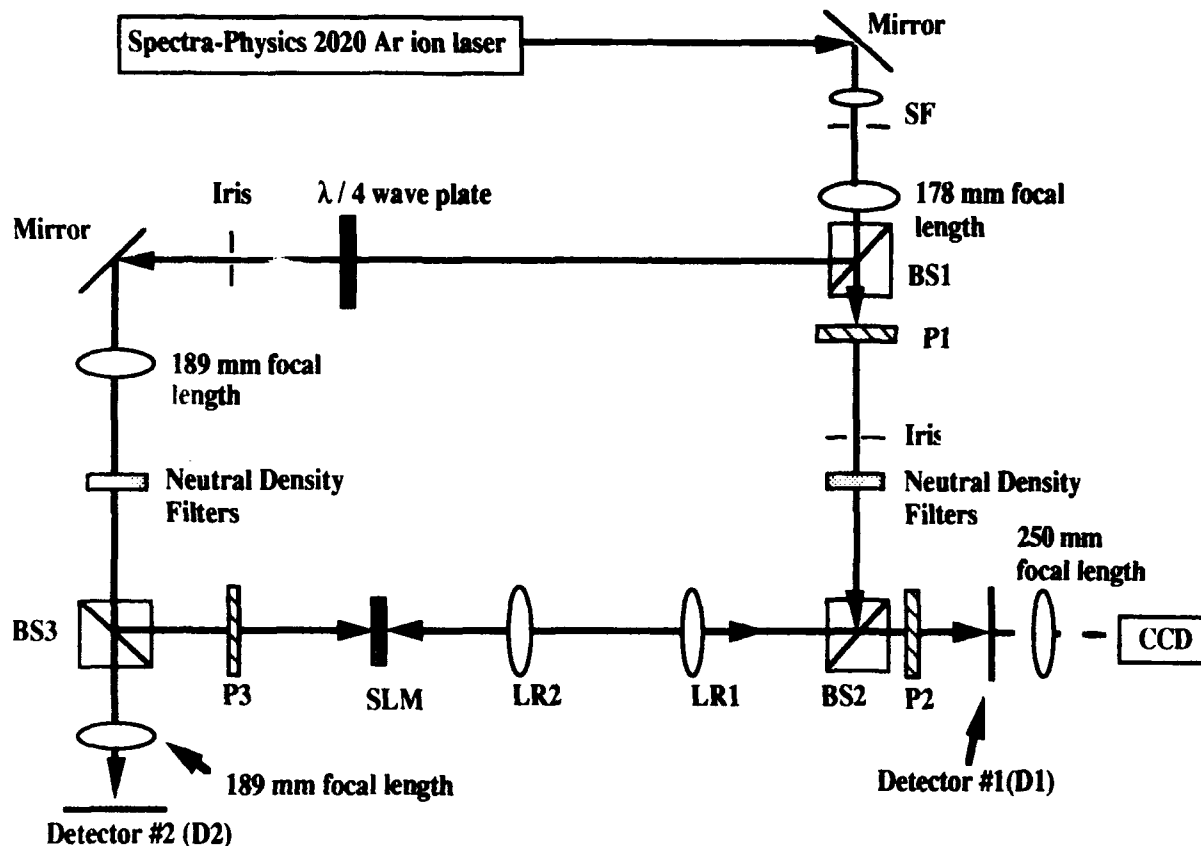


Figure 18. Experimental System Used to Measure Response of LCLV with Green Read Illumination.

(Published with permission from Janine Reardon, UAH Center for Applied Optics, Huntsville, AL.)

The write beam path consisted of a $\lambda/4$ plate, iris, steering mirror, two 189 mm focal length lenses, neutral density holder and filters, a polarizing beamsplitter, rotatable polarizer, and a silicon photodetector. A 189 mm focal length lens was used to image the iris diaphragm onto the write surface of the SLM via beamsplitter BS3. The $\lambda/4$ plate was oriented for optimum beam reflection at BS3 onto the surface of the SLM. The transmitted beam of BS3 was collimated by the second 189 mm focal length lens before incidence on an NRC model 818-SL photodetector. Polarizer P3 was oriented to assure vertical polarization incident on the write surface of the SLM. A calibration test series was performed to determine the relationship between write light intensities measured at plane D2 and at the write surface of the LCLV. The LCLV was temporarily replaced with a second photodetector and the output of the two photodetectors was recorded for various neutral density filters inserted in filter holder #2.

The read beam path consisted of two rotatable polarizers, iris, neutral density holder and filters, polarizing beamsplitter, two lenses (focal lengths of 178 and 300 mm), and a silicon photodetector. Polarizer P1 was oriented to preferentially pass vertically polarized light. The iris diaphragm was imaged by lens LR1, a 178 mm focal length biconvex lens, at an intermediate plane between lenses LR1 and LR2. Lens LR2, a 300 mm focal length biconvex, was utilized to effectively collimate the beam incident on the read surface of the SLM. Upon reflection from the read surface of the LCLV, lenses LR2 and LR1 were used to effectively image the modulated read beam onto the photodetector D1. Polarizer P2 was oriented for optimum image visibility at detector plane D1. Optimum visibility was determined by temporary removal of detector D1 and using a 250 mm focal length lens to image the modulated beam on a CCD located at the CCD plane shown in Figure 18. The neutral density filters and holder in the read beam served a twofold purpose. First, the filters were used to calibrate the amount of light incident on the read surface of the SLM with respect to the light transmitted by BS2. Secondly, the filters were used to calibrate the amount of light transmitted by BS2 with respect to the light transversing the read beam path and incident on detector D1 when the SLM was replaced by a mirror. Third, the filters were used to attenuate the light incident on the read surface of the SLM.

Initially, the iris diaphragm was imaged onto the write surface of the LCLV. The image of the iris was then partially blocked to allow for a half-bright and half-dark image written to the LCLV. The driving waveform, amplitude, and frequency, as well as the orientation of the analyzer P2 were varied until an image of optimal visibility was observed at detector plane D1. The silicon photodetector located in this plane was temporarily removed for imaging of the modulated read beam at the CCD plane. The optimum driving signal for the LCLV was again determined to be a 1.92 KHz sinusoid with an amplitude of 9.96 volts. This image corresponded to a write light intensity of 0.9 mW/cm^2 incident on the SLM. The driving frequency was again reduced to 1.0 KHz.

The silicon photodetector was repositioned at plane D1 and the neutral density filters of filter holder #2 varied over an extended range. The read and write intensities of detector D1 and D2, respectively, were recorded as the write light incident on the LCLV was altered. The resultant response of the LCLV modulated read beam as a function of write light intensity is shown in Figure 19. Data was also taken for driving frequencies of 2 KHz and 5 KHz. Analyzer P2 was adjusted at the beginning of each data run to achieve an image of optimal visibility at detector D1, and thus at the CCD plane, for a write light intensity of 0.9 mW/cm^2 incident on the SLM. The resulting data is plotted with the 1 KHz frequency data in Figure 19.

Next, the response of the LCLV was measured as a function of the driving amplitude. Again, the read and write beam intensities were recorded as the write light incident on the LCLV was altered. Initially, the LCLV was operated with a 1.92 KHz 10 V sinusoidal driving signal. Analyzer P2 was oriented for optimum image visibility at an incident write light intensity of 0.9 mW/cm^2 . Data for driving amplitudes of 8, 10, and 12 V are shown graphically in Figure 4.6.

1.0 KHz case:

$$I_r = 181 \left\{ 1 - \exp \left(\frac{-I_w}{5.35} \right) \right\} - 3.70$$

2.0 KHz case:

$$I_r = 180 \left\{ 1 - \exp \left(\frac{-I_w}{8.34} \right) \right\} - 3.49$$

5.0 KHz case:

$$I_r = 175 \left\{ 1 - \exp \left(\frac{-I_w}{18.2} \right) \right\} - 2.56$$

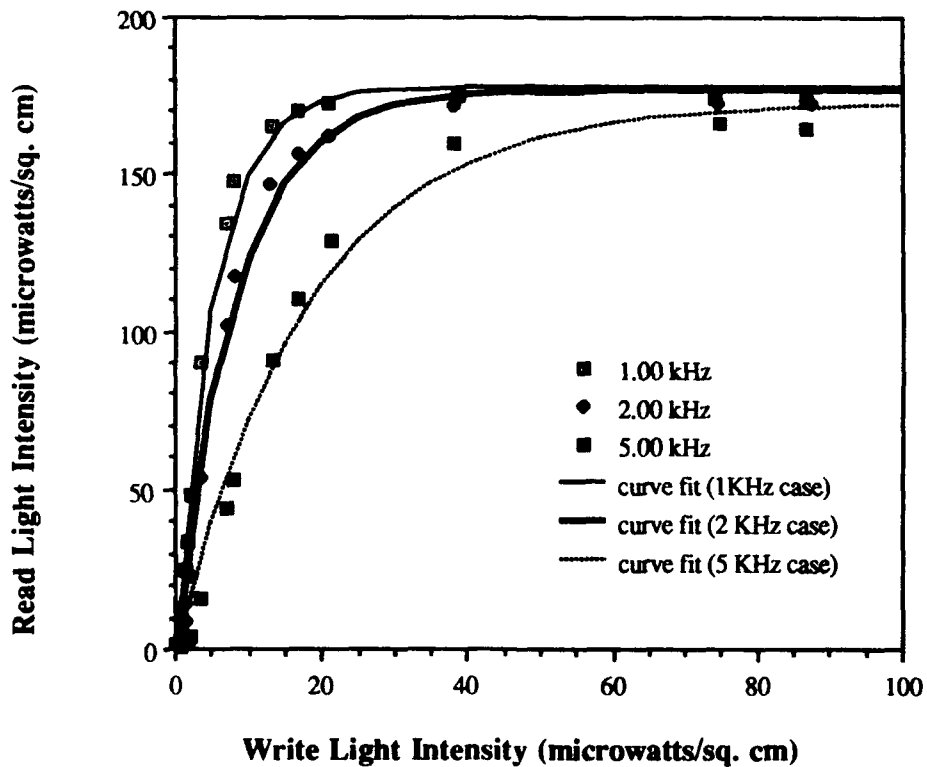


Figure 19. Response of Hughes LCLV to Driving Frequency for Green (514.5 nm) Write and Read Beams

(Published with permission of Janine Reardon, University of Alabama in Huntsville.)

8.0 V case:

$$I_r = 253 \left\{ 1 - \exp \left(\frac{-I_w}{79.3} \right) \right\} - 0.859$$

10.0 V case:

$$I_r = 174 \left\{ 1 - \exp \left(\frac{-I_w}{8.31} \right) \right\} - 3.28$$

12.0 V case:

$$I_r = 196 \left\{ 1 - \exp \left(\frac{-I_w}{2.40} \right) \right\} - 4.96$$

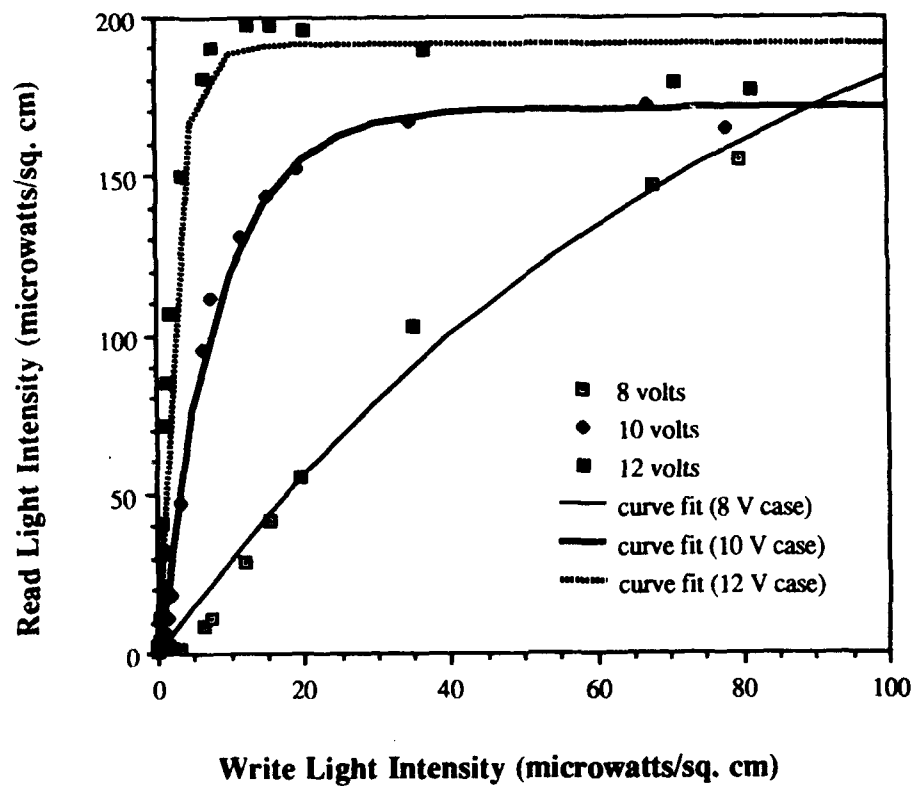


Figure 20. Response of Hughes LCLV to Driving Amplitude for Green (514.5 nm) Write and Read Beams

(Published with permission of Janine Reardon, University of Alabama in Huntsville.)

V. GEC-MARCONI SLM RESPONSE

The experimental system shown in Figure 21 was used to measure the response of an optically addressed SLM from GEC-Marconi as a function of write light intensity for various driving waveforms and amplitudes while maintaining a fixed spectral addressing of red ($\lambda=632.8$ nm) read beam and a green ($\lambda=514.5$ nm) write beam. This system is similar to the one discussed in Section IV for the Hughes LCLV. A Spectra-Physics model 124B HeNe laser was spatially filtered and collimated using standard laboratory techniques. A polarizer was used, as discussed in Section IV, to selectively address the read surface of the GEC-Marconi SLM with vertically polarized light via a nonpolarizing beam splitter. Polarizer P3 was used as an analyzer of the modulated read beam to observe an optimal amplitude modulated image at detector plane D2 via lens L3. L3 was biconvex lens with a focal length of 254 mm and detector D2 was a Newport Research Corporation (NRC) model 818SL silicon photodetector mated to an NRC model 835 power meter. The neutral density filters in the read beam were used to attenuate the light incident on the read surface of the GEC-Marconi SLM. The light incident upon this surface was measured to be approximately $8 \mu\text{W}/\text{cm}^2$. The write beam to the SLM was constructed from a Spectra-Physics model 2020 argon ion laser source. Polarizer P1 was used to preferentially address the

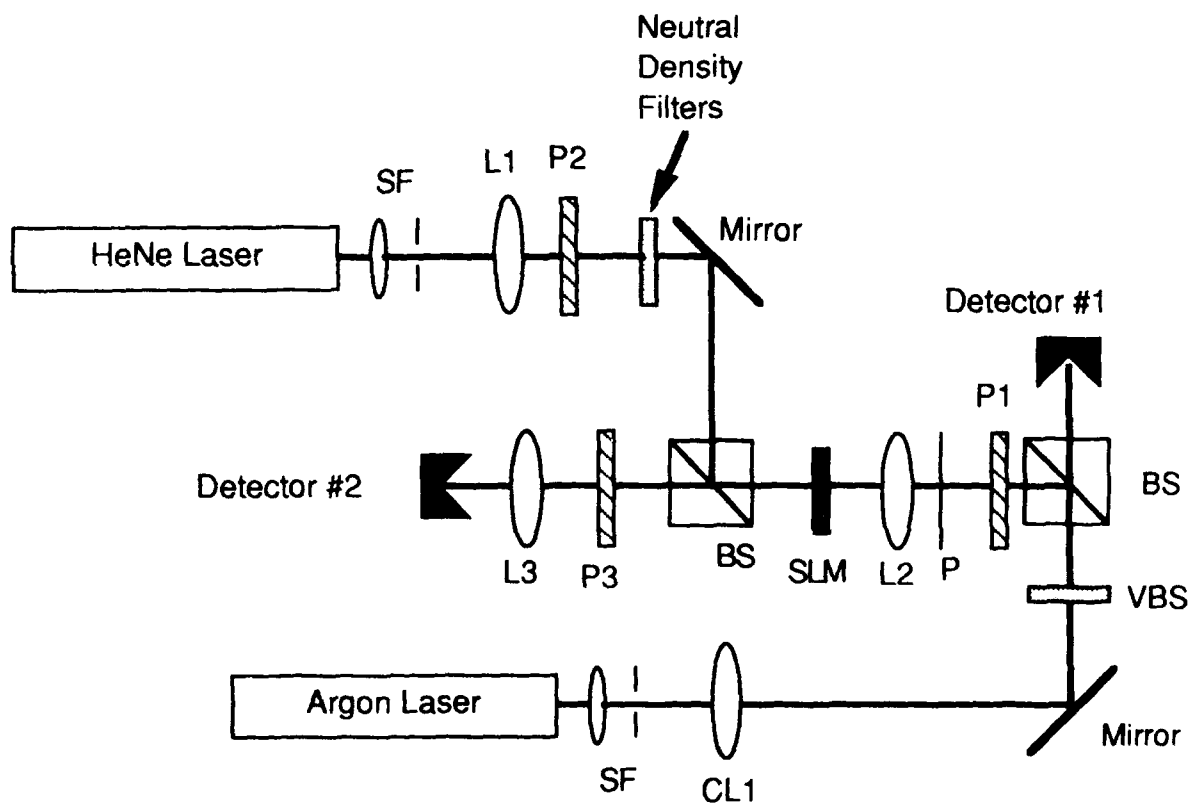


Figure 21. Experimental System Used to Measure Response of GEM-Marconi SLM with Red Read Illumination

write surface of the SLM with vertically polarized light via a nonpolarizing beamsplitter. A variable beamsplitter/attenuator was inserted in the write beam prior to the nonpolarizing beamsplitter to provide a means of varying the write light intensity incident on the write surface of the SLM and the reference write beam photodetector D1. Detector D1 was a NRC model 818SL silicon photodetector mated to a NRC model 815 power meter.

Initially, a USAF resolution transparency was imaged onto the write surface of the SLM via lens L2, a compound imaging lens with an effective focal length of 50 mm. The driving waveform, amplitude, and frequency, as well as the orientation of the analyzer P3, were varied until an image of optimal visibility was observed at detector plane D2. The silicon photodetector/power meter located in this plane was temporarily replaced with a CCD camera to observe the modulated read beam image. The optimum driving signal for the GEC-Marconi SLM was determined to be a 1.1 KHz sinusoid with an amplitude of 3.1 volts. This image corresponded to a write light intensity of $300 \mu\text{W}/\text{cm}^2$ incident on the SLM.

The silicon photodetector was repositioned at plane D2 and the variable attenuator rotated over an extended range. The read and write intensities of detector D2 and D1, respectively, were recorded as the write light incident on the GEC-Marconi SLM was altered. The resultant response of the SLM's modulated read beam as a function of write light intensity is shown in Figure 22. Data was also measured for driving voltages of 2.6 V and 3.6 V. Analyzer P3 was adjusted at the beginning of each data run to achieve an image of optimal visibility at detector D2 for a write light intensity of $300 \mu\text{W}/\text{cm}^2$ incident on the SLM. The resulting data is plotted with the 3.1 V amplitude data in Figure 22.

Next, the response of the GEC-Marconi SLM was measured as a function of the driving frequency. Again, the read and write beam intensities were recorded as the write light incident on the SLM was altered. Initially, the SLM was operated with a 1.0 KHz 3.1 V sinusoidal driving signal. Analyzer P3 was oriented for optimum image visibility at an incident write light intensity of $300 \mu\text{W}/\text{cm}^2$. Data runs for driving frequencies of 1, 2, and 0.5 KHz are shown graphically in Figure 23.

The data presented in Figures 22 and 23 were taken from the least amount of write light incident on the SLM to the most intense amount of light. Concern was expressed that the SLM may respond differently to the write light intensity if this sequence was reversed – from the most to least intense write light incident on the GEC-Marconi SLM. The SLM was tuned for optimal image visibility with a 1.1 KHz, 3.1 V amplitude sine wave with an incident write light intensity of $300 \mu\text{W}/\text{cm}^2$. Two data runs were performed with this driving waveform. Initially, the variable beamsplitter/attenuator was adjusted from the least to most intense write light incident on the SLM write surface while the modulated read beam intensity from detector D2 was recorded. Then the attenuator was adjusted from the most to least intense write beam incident on the SLM while the intensity of the modulated read beam was recorded. These two data runs are depicted graphically in Figure 24. As shown by Figure 24, the GEC-Marconi SLM did not respond differently regardless of the order in which the write light intensity was varied.

2.6 V case:

$$I_r = 0.124 \left\{ 1 - \exp \left(\frac{-I_w}{289} \right) \right\} + 0.0646$$

3.1 V case:

$$I_r = 0.272 \left\{ 1 - \exp \left(\frac{-I_w}{252} \right) \right\} + 0.133$$

3.6 V case:

$$I_r = 0.399 \left\{ 1 - \exp \left(\frac{-I_w}{208} \right) \right\} + 0.178$$

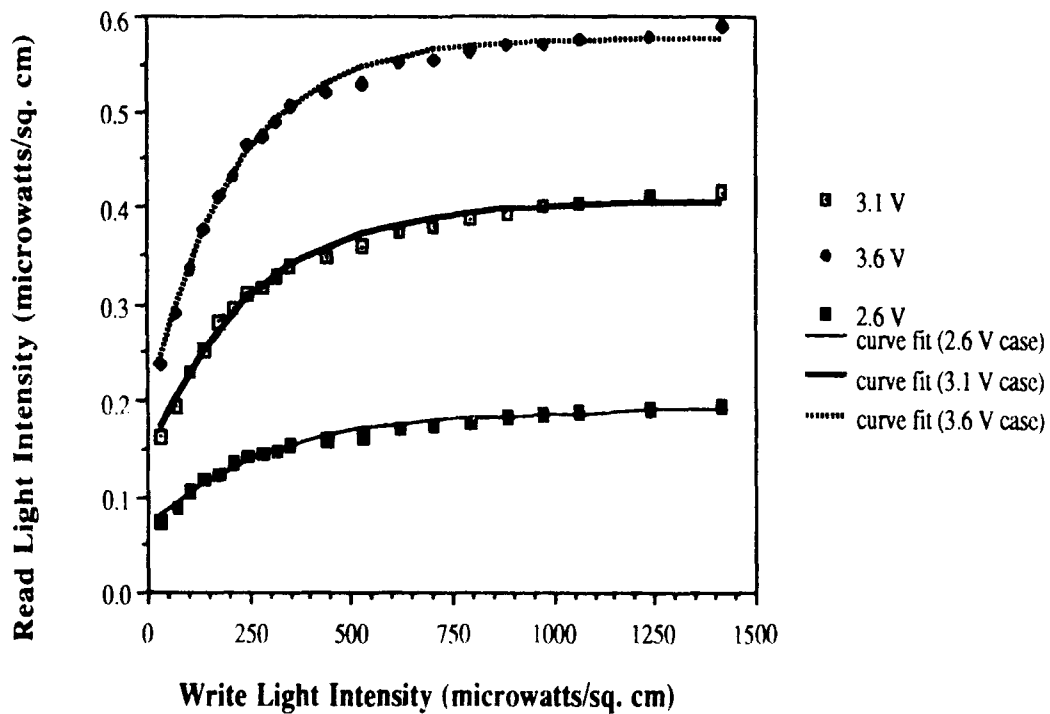


Figure 22. Response of GEC-Marconi SIM to Driving Amplitude with Optimization of Visibility Per Amplitude

0.5 KHz case:

$$I_r = 0.297 \left\{ 1 - \exp \left(\frac{-I_w}{130} \right) \right\} + 0.225$$

1.0 KHz case:

$$I_r = 0.272 \left\{ 1 - \exp \left(\frac{-I_w}{252} \right) \right\} + 0.133$$

2.0 KHz case:

$$I_r = 0.226 \left\{ 1 - \exp \left(\frac{-I_w}{440} \right) \right\} + 0.057$$

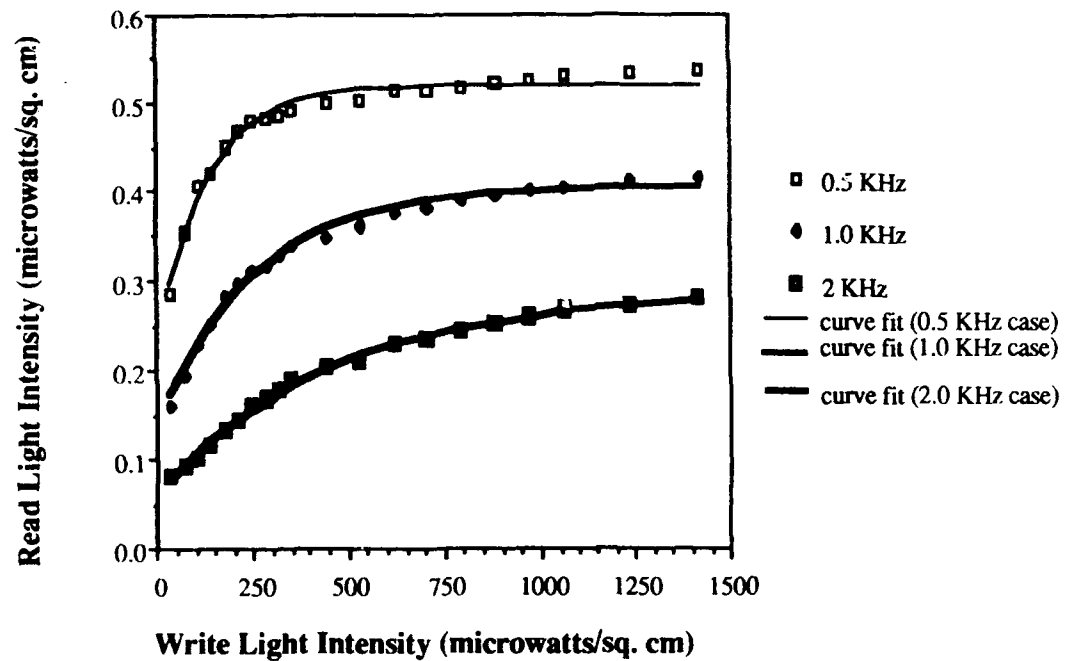


Figure 23. Response of GEC-Marconi SLM to Driving Frequency with Optimization of Visibility Per Frequency

Any nonlinear response of the two photodetectors D1 and D2 could have negated the nonlinearity shown in Figures 22-24. The SLM was removed from the system and neutral density filters inserted in the SLM location. These filters were used to attenuate the transmitted write beam to an intensity level comparable to the SLM's modulated read beam that was normally incident on detector D2. The attenuator in the write beam was adjusted over the range of write light intensities used to collect the data of Figures 22-24 and detectors D1 and D2 readings were recorded. The resulting data is depicted in Figure 25. The response of the detectors with respect to each other is approximately linear over the range of light intensities used in the above analysis with the GEC-Marconi SLM.

The SLM was then reinserted in the experimental system depicted in Figure 21. The modulated read beam image visibility was optimized by rotation of analyzer P3 while the modulator was addressed with a $300 \mu\text{W}/\text{cm}^2$ write light intensity and driven by a 1.1 KHz, 3.1 V amplitude sine wave. The optimum visibility was qualitatively determined by insertion of a USAF resolution chart in the write beam and viewing the modulated read beam by temporarily replacing detector D2 with a CCD camera. Thereafter, the USAF chart was removed and the camera replaced with detector D2. The visibility was calculated by recording the readings of detector D2 with the write beam blocked and unblocked. The background or zero of D2 was determined by temporarily blocking the detector and recording the reading. Optimum visibility by this method was calculated

1.0 KHz case (run #1):

$$I_r = 0.294 \left\{ 1 - \exp\left(\frac{-I_w}{212}\right) \right\} + 0.080$$

1.0 KHz case (run #2):

$$I_r = 0.288 \left\{ 1 - \exp\left(\frac{-I_w}{211}\right) \right\} + 0.0797$$

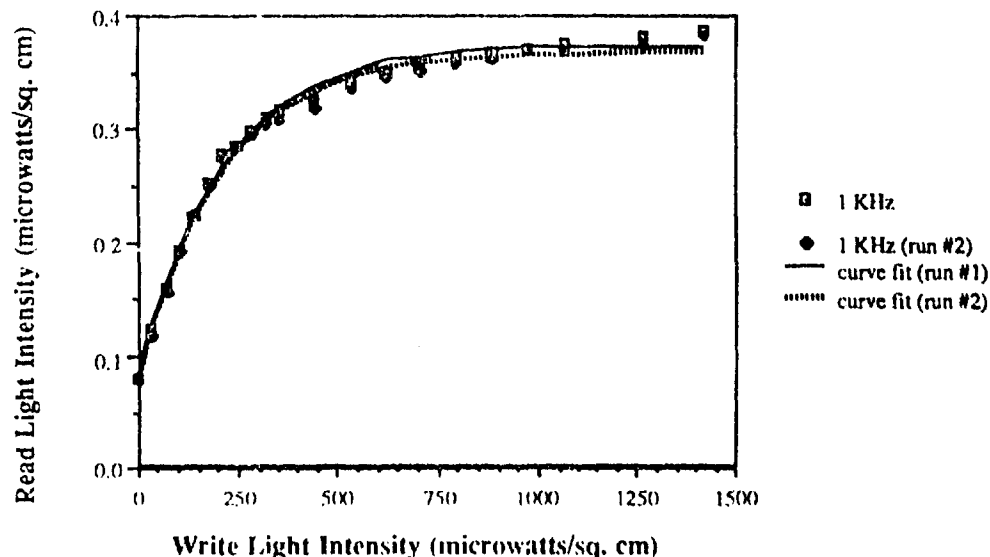


Figure 24. Response of GEC-Marconi SLM to Order of Write Light Intensity Addressing

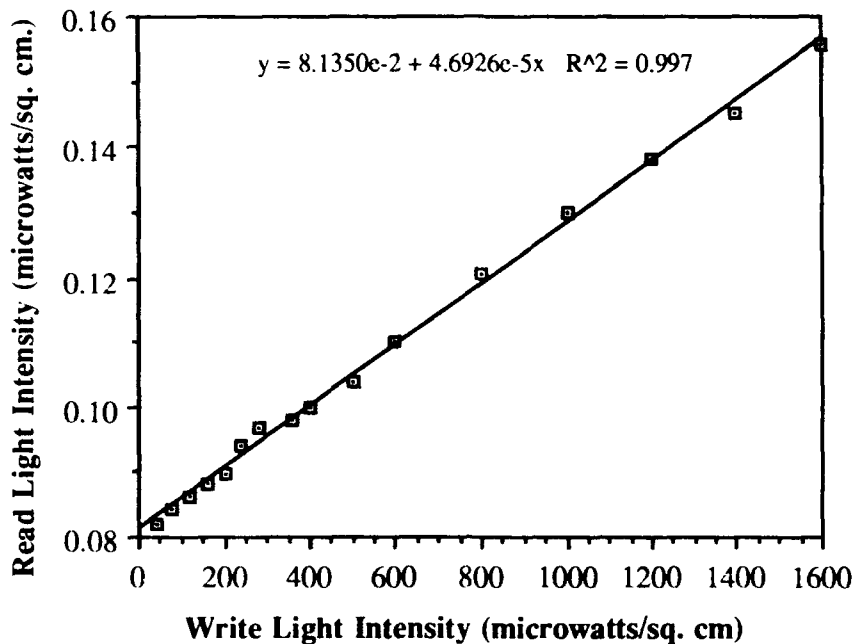


Figure 25. Response of Photodetectors with Respect to Each Other

to be 0.60. Data of read and write beam intensities were recorded as the attenuation in the write beam was changed. The resulting data is shown in Figure 26.

The response of the modulated read beam was also recorded as a function of write light intensity for frequencies of 0.5 and 2 KHz. The output analyzer was not adjusted to obtain an optimum image visibility for $300 \mu\text{W}/\text{cm}^2$ incident write light for each of these frequencies. Instead, the visibility was measured as described above for the analyzer orientation that was determined to be optimum for the initial 1.1 KHz, 3.1 V sine wave for each of these frequencies. Visibility was determined to be 0.53 and 0.63 for the 0.5 and 2 KHz frequencies of SLM operation, respectively. The response of the modulated read beam as a function of write light intensity was measured and the results are graphed in Figure 26.

Next, the driving waveforms amplitude was varied and the response of the read beam, as a function of write light intensity, was recorded for the GEC-Marconi SLM. Again, the output analyzer P3 was not adjusted between variations of the driving amplitude. The response of the read beam as a function of write light intensity was measured for 2.6 V and 3.6 V amplitudes of the 1.1 KHz sine wave in addition to the initial 3.1 V amplitude. The visibility was calculated by the methods discussed above for each of these driving amplitudes while utilizing an incident write light of $300 \mu\text{W}/\text{cm}^2$ on the SLM surface. These visibilities corresponded to 0.69 and 0.51 for the 2.6 and 3.6 V amplitudes, respectively. The resultant response of the GEC-Marconi SLM to variations in write light intensities and driving waveform amplitudes is depicted graphically in Figure 27.

0.5 KHz case:

$$I_r = 0.277 \left\{ 1 - \exp \left(\frac{-I_w}{118} \right) \right\} + 0.196$$

1.0 KHz case:

$$I_r = 0.294 \left\{ 1 - \exp \left(\frac{-I_w}{212} \right) \right\} + 0.080$$

2.0 KHz case:

$$I_r = 0.215 \left\{ 1 - \exp \left(\frac{-I_w}{412} \right) \right\} + 0.051$$

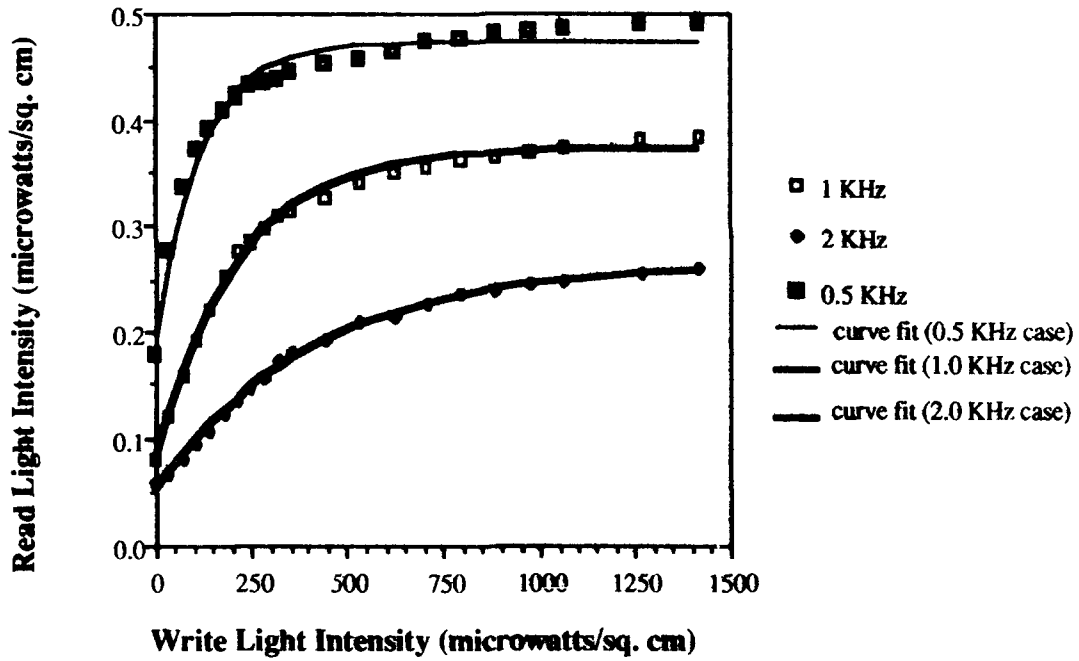


Figure 26. Response of GEC-Marconi SLM to Driving Frequency with Optimization of Visibility at 1.1 KHz.

2.6 V case:

$$I_r = 0.124 \left\{ 1 - \exp \left(\frac{-I_w}{275} \right) \right\} + 0.03907$$

3.1 V case:

$$I_r = 0.2298 \left\{ 1 - \exp \left(\frac{-I_w}{207} \right) \right\} + 0.0698$$

3.6 V case:

$$I_r = 0.307 \left\{ 1 - \exp \left(\frac{-I_w}{203} \right) \right\} + 0.115$$

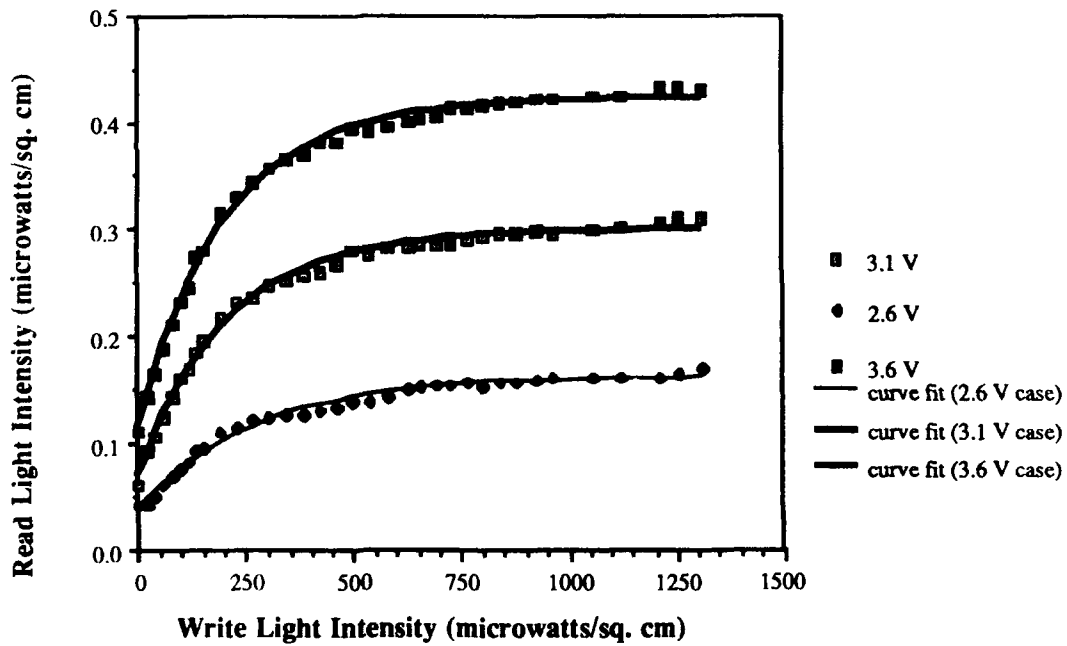


Figure 27. Response of GEC-Marconi SLM to Driving Amplitude with Optimization of Visibility at 3.1 V

VI. FLC SLM RESPONSE

The experimental system shown in Figure 28 was used to measure the response of an optically addressed FLC SLM from the University of Colorado-Boulder as a function of write light intensity for various driving waveforms and amplitudes while maintaining a fixed spectral addressing of red ($\lambda=632.8$ nm) read beam and a green ($\lambda=514.5$ nm) write beam. This system is similar to the ones discussed in Section IV for the Hughes LCLV and Section 5 for the GEC-Marconi SLM. A Spectra-Physics model 124B HeNe laser was spatially filtered and collimated using standard laboratory techniques. A polarizer was then used to selectively address the read surface of the FLC SLM with vertically polarized light via a nonpolarizing beamsplitter. Polarizer P3 was used as an analyzer of the modulated read beam to observe an optimum amplitude modulated image at detector plane D2 via lens L3. L3 was biconvex lens with a focal length of 254 mm and detector D2 was a Newport Research Corporation (NRC) model 818SL silicon photodetector mated to an NRC model 835 power meter. The neutral density filters in the read beam were used to attenuate the light incident on the read surface of the FLC SLM. The light incident upon this surface was measured to be approximately $8 \mu\text{W}/\text{cm}^2$. The write beam to the SLM was constructed from a Spectra-Physics model 2020 argon ion laser source. Polarizer P1 was used to preferentially address the write surface of the SLM with vertically polarized light via a nonpolarizing beamsplitter. A variable beamsplitter/attenuator was inserted in the write beam prior

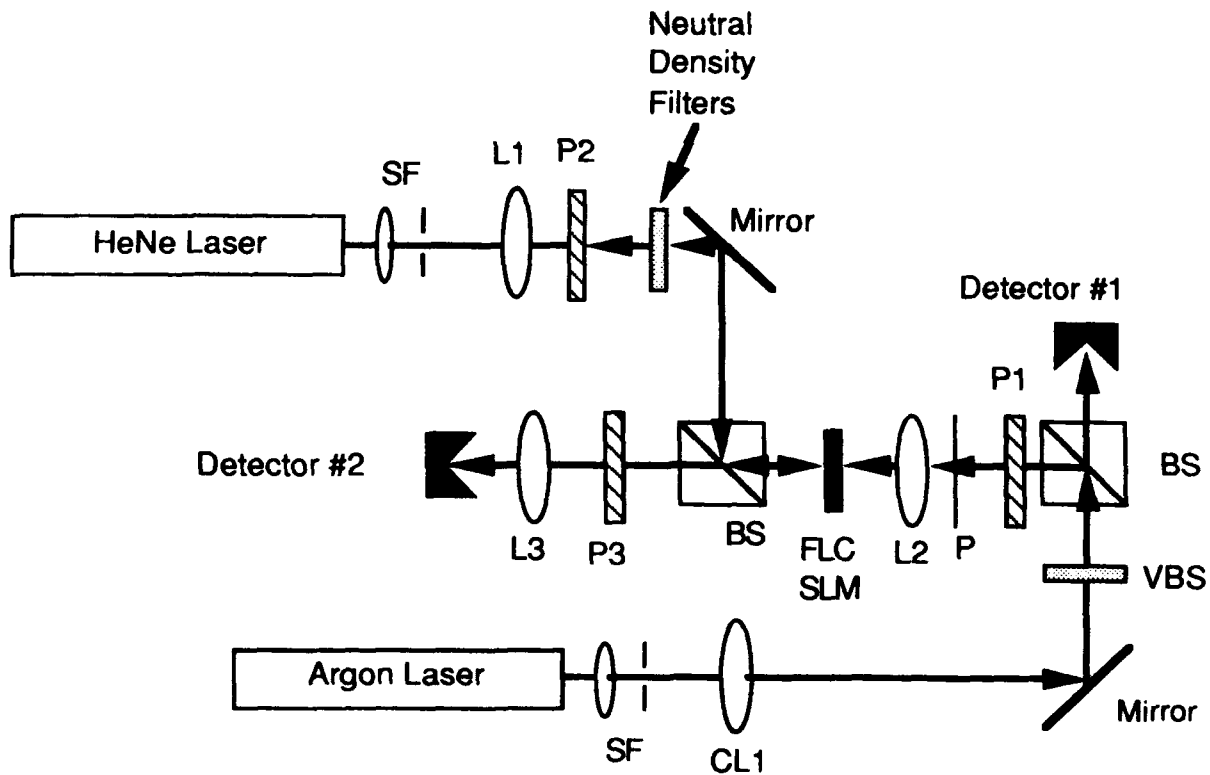


Figure 28. Experimental System Used to Measure Response of FLC SLM with Red Read Illumination

to the nonpolarizing beamsplitter to provide a means of varying the write light intensity incident on the write surface of the SLM and the reference write beam photodetector D1. Detector D1 was an NRC model 818SL silicon photodetector mated to an NRC model 815 power meter.

Initially, a USAF resolution transparency was imaged onto the write surface of the SLM via lens L2, a compound imaging lens with an effective focal length of 50 mm. The driving waveform, amplitude, and frequency, as well as the orientation of the analyzer P3 were varied until an image of optimum visibility was observed at detector plane D2. The silicon photodetector/power meter located in this plane was temporarily replaced with a CCD camera to observe the modulated read beam image. The optimum driving signal for the optically addressed FLC SLM was determined to be a 1.0 KHz square wave with a peak-to-peak voltage of 24 V and a DC offset of -2 V. This image corresponded to a write light intensity of $300 \mu\text{W}/\text{cm}^2$ incident on the SLM. The visibility of the image was measured by repositioning the silicon photodetector at plane D2 and recording the relative intensity of the modulated read beam as the write beam was blocked and unblocked from addressing the write surface of the FLC SLM. The visibility was determined to be 0.72.

The variable attenuator was then rotated over an extended range. The read and write intensities of detector D2 and D1, respectively, were recorded as the write light incident on the FLC SLM was altered. The resultant response of the SLM's modulated read beam as a function of write light intensity for the optimum driving waveform discussed above is shown in Figure 29. Data was also recorded over an extended driving waveform amplitude range. This data was collected for peak-to-peak voltages from 21 to 24 V in one volt increments while maintaining the DC offset of -2 V. Analyzer P3 was adjusted at the beginning of each data run to achieve an image of optimum visibility at detector D2 for a write light intensity of $300 \mu\text{W}/\text{cm}^2$ incident on the SLM. The resulting data is plotted along with the 24 V_{p-p} data above in Figure 30.

Next, the response of the FLC SLM was measured as a function of the driving frequency. The read and write beam intensities were observed as the write light incident on the SLM was altered. Initially, the FLC was driven with the optimum driving waveform discussed above. Analyzer P3 was oriented for optimum image visibility at an incident write light intensity of $300 \mu\text{W}/\text{cm}^2$. The response of the FLC SLM did not vary with driving frequencies from 500 Hz to 5 KHz. The driving waveform voltage was then detuned to 22 V_{p-p} and the response as a function of frequency was observed. Again, the variation in frequency did not significantly alter the response of the FLC SLM.

The above data corresponds to operation of the FLC SLM in an amplitude modulating or 'maximum contrast' mode. Data was also collected when the FLC SLM was operated in a binary phase or 'phase-only' mode. This 'phase-only' mode was determined by imaging the USAF resolution chart onto the write surface of the FLC SLM and adjusting polarizer P3 until ideally no apparent contrast in the modulated read beam image was evident at detector D2. Although the contrast of the read beam was minimized, some amplitude modulation was evident in the read beam. This state occurred at the mid-point between maximum contrast and maximum reverse contrast states. The chart was then removed and the read and write beam intensities were recorded for various write beam intensities at the optimal driving signal. The results are shown in Figure 31.

24 Vp-p case:

$$I_r = .040658 - 1.5609 \times 10^{-4} \cdot I_w + 1.0769 \times 10^{-6} \cdot I_w^2 - 7.8348 \times 10^{-10} \cdot I_w^3 ;$$
$$R^2 = 0.994$$

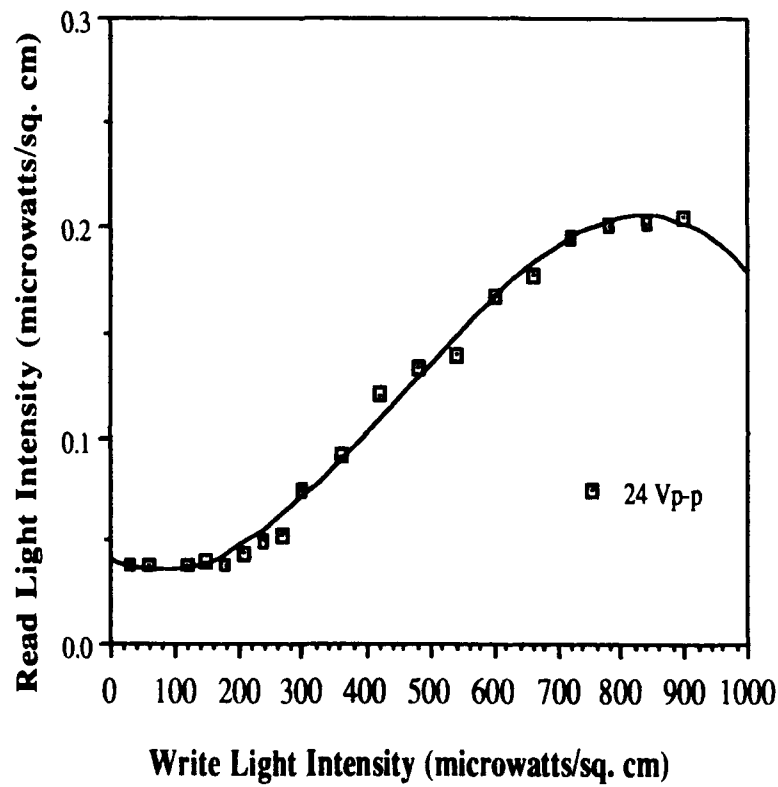


Figure 29. FLC SLM Response at Optimal Driving Waveform

21 Vp-p case:

$$I_r = -0.00164 + 4.6887 \times 10^{-4} \cdot I_w - 5.5893 \times 10^{-7} \cdot I_w^2 + 1.9956 \times 10^{-10} \cdot I_w^3 ;$$

$$R^2 = 0.985$$

22 Vp-p case:

$$I_r = 0.02442 + 4.6449 \times 10^{-4} \cdot I_w - 6.943 \times 10^{-7} \cdot I_w^2 + 3.5261 \times 10^{-10} \cdot I_w^3 ;$$

$$R^2 = 0.996$$

23 Vp-p case:

$$I_r = 0.018053 + 5.1095 \times 10^{-4} \cdot I_w - 7.9547 \times 10^{-7} \cdot I_w^2 + 3.9949 \times 10^{-10} \cdot I_w^3 ;$$

$$R^2 = 0.976$$

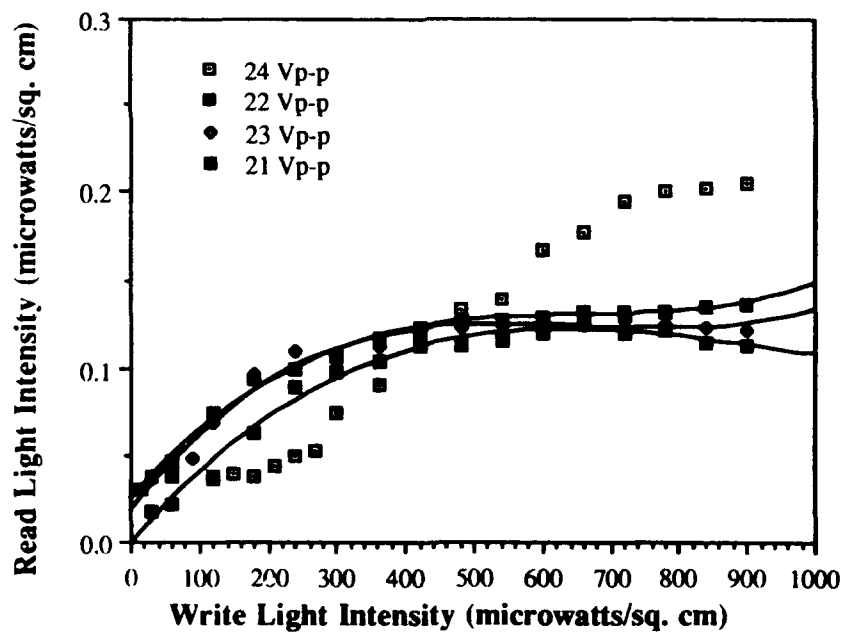


Figure 30. FLC SLM Response as a Function of Voltage

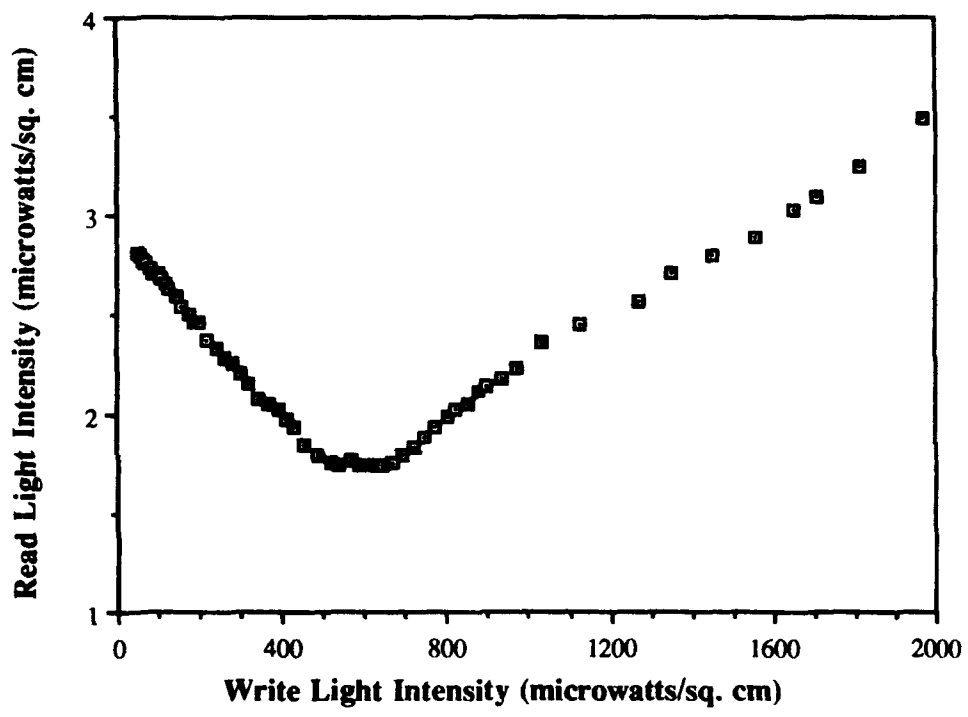


Figure 31. Binary Phase Operation FLC SLM Response

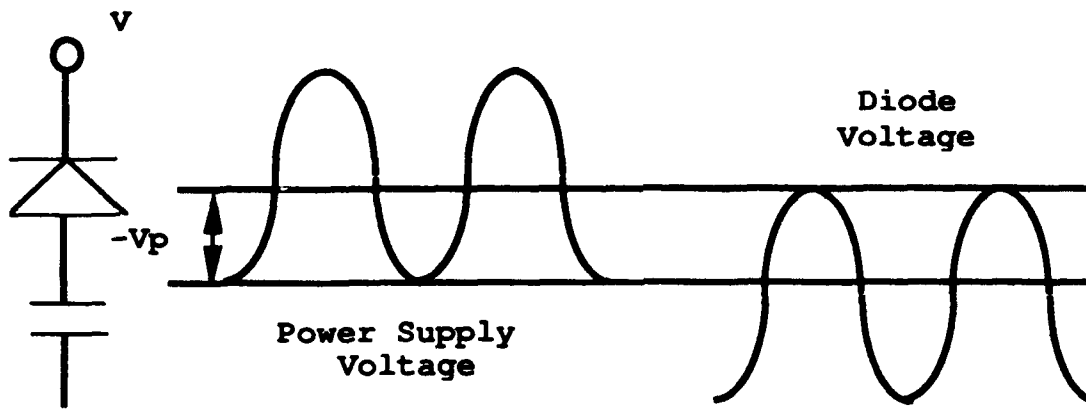
VII. SLM EQUIVALENT CIRCUIT MODELS

The data representing the behavior of several SLMs presented in the preceding sections may be best understood by analyzing their equivalent electrical circuit models. The models presented have been previously discussed in the literature [24-27]. However, the analysis of these equivalent circuits for the behavior described in Sections IV-VI is unique.

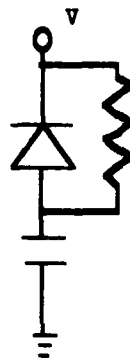
A. Hughes Liquid Crystal Light Valve (LCLV)

The electrical circuit models for the Hughes LCLV, as well as the GEC-Marconi SLM and the FLC SLM, are essentially composed of two parallel RC circuits. One parallel RC circuit is used to model the behavior of the liquid crystal material - either twisted nematic or ferroelectric. The second parallel RC circuit, in conjunction with a diode, is used to model the behavior of the photosensor. Following Grinberg [28], the operation of the Hughes LCLV may best be understood by first discussing an idealistic equivalent circuit for the LCLV photosensor, the CdTe light blocking layer, and the dielectric mirror. This simple circuit consists of a diode in series with a capacitor. The diode represents the junction formed between the CdS photosensor and the CdTe layer, and the capacitor represents the capacitance of the dielectric mirror. For completeness, the dielectric mirror may also be modelled as a parallel RC circuit. However, the resistance of the dielectric mirror is high for most practical mirror constructions and can thus be ignored. The equivalent circuit for the CdS/CdTe layers and dielectric mirror is shown in Figure 32(a) for the case of no input (write light) illumination. When an ac voltage is applied to this circuit, the capacitor will be charged during the first cycle to the negative peak voltage, depicted as $-V_p$. This voltage then serves as a reverse bias voltage on the diode for all values of the ac voltage. Assuming ideal diode behavior (i.e., infinite back resistance for the diode), the steady state current flow in this circuit is then zero, regardless of the driving waveforms characteristics (amplitude, frequency, and waveform, if periodic). Figure 32(b) represented the equivalent circuit for the CdS/CdTe layers and dielectric mirror when input illumination is present. The photons of the incident light introduces a leakage resistance across the diode. This resistance discharges the capacitor during the reverse bias cycle of the diode. The approximate waveform response is shown in Figure 32(c). If the operating frequency is slow enough or the current high enough, the liquid crystal material will be driven above its electro-optic threshold by the field developed across it.

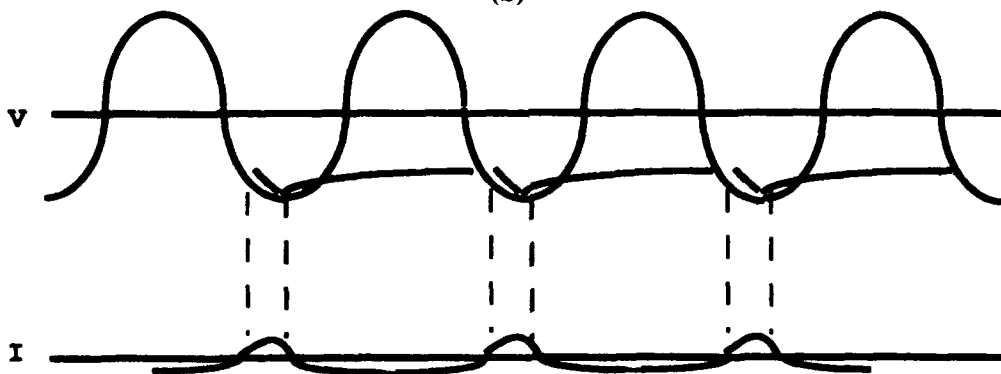
The more realistic circuit model for the Hughes LCLV is shown in Figure 33. In this circuit, R_{lc} and C_{lc} represent the resistance and capacitance of the twisted nematic liquid crystal, C_m represents the capacitance of the dielectric mirror, R_{fd} , $R_{fd}+R_{bd}$, and C_d represent the forward resistance, reverse resistance, and capacitance of the photodiode representing the CdS/CdTe layer. The leakage resistance of the dielectric mirror, R_m , is usually high and has been neglected in this circuit model. The equivalent circuit shown will pass current whether the photosensor is illuminated or not. However, the illumination decreases the values of R_{fd} and R_{bd} . As a result, the current flow in the illuminated region is greater than the nonilluminated regions of the photosensor. This difference in current flow provides a method of controlling the electro-optic effect of the nematic liquid crystal with the photosensor. The CdS/CdTe layer, in conjunction with the dielectric mirror, is designed so that the current flow in the nonilluminated region is less than the liquid



(a)



(b)



(c)

Figure 32. Equivalent Circuits for (a) Ideal Light Valve Without Write Light Illumination, (b) Ideal Light Valve with Write Light Illumination, and (c) Equivalent Circuit Voltage and Current Waveforms of an Ideal Light Valve

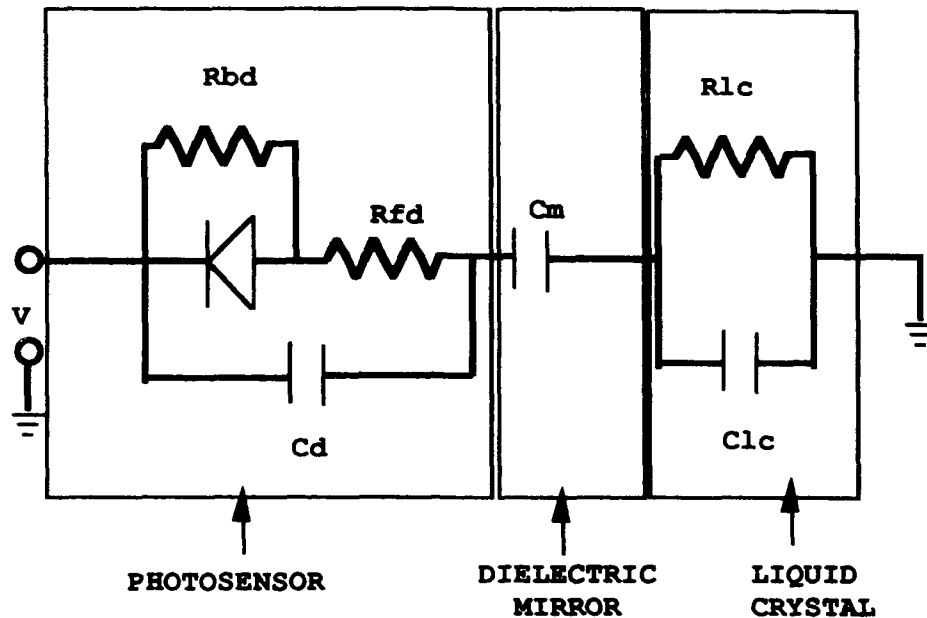


Figure 33. Circuit Model for Hughes LCLV

crystal's threshold while the current flow in the illuminated region is greater than the liquid crystal's threshold level. The electro-optic effects of the liquid crystal material in a 90 degree twisted cell configuration was discussed in Section II and will not be restated here.

The response time data of the Hughes LCLV, given in Section III, verifies the depiction of the twisted nematic liquid crystal material as a simple parallel RC circuit. When the illumination is terminated, the response of the LCLV decays in a manner consistent with the discharge of an RC filter, and the response of the LCLV is characteristic of the charging time of an RC filter when the photosensor is illuminated.

The response of the LCLV modulated read beam to variations in write light intensity was given in Section IV. This behavior was measured as a function of frequency and amplitude of the driving waveform. The response of the LCLV maintained similar characteristic shapes for various driving frequencies. This response can best be explained by an analysis using the circuit model of Figure 33. For a given driving waveform frequency, the resistance of the photodiode is decreased for increasing write light intensities. This results in more current flowing through the photosensor, and consequently the liquid crystal layer. The field across the complete device remains constant. Therefore as the photodiode passes more current to the liquid crystal layer, a larger amount of voltage is dropped across it. This increase in voltage across the liquid crystal layer results in a more complete reorientation of the elongated liquid crystal molecules normal to the electrode surface. If all the molecules were to become normal to the electrode surfaces, a dark on-state would occur with the crossed polarizer/analyzer pair because the polarization of the light would not be altered by the liquid crystals due to their molecular orientation. However, a voltage

regime exists where the LCLV transmits light between the "full-on" and "full-off" states. The optical birefringence of the molecules affects the polarization of the light between the parallel and perpendicular orientations of the molecules with respect to the electrode surfaces. As a result, the light that emerges from the LCLV at these intermediate voltage levels (across the liquid crystal) is no longer linearly polarized, so that some transmission through the analyzer may occur. The amount of light transmitted is a function of the amount of voltage dropped across the liquid crystal layer; however, the voltage dropped across the liquid crystal is not linear with respect to the input write illumination due to the characteristics of the photodiode. The ideal response of a diode is shown in Figure 34, along with the typical response of Ge and Si diodes [29]. The amount of current passed by the diode configuration is nonlinear with respect to the input illumination. This nonlinearity was observed in the response behaviors detailed in Sections IV–VI. However, there exists an illumination regime where the diode essentially passes any further increases in current

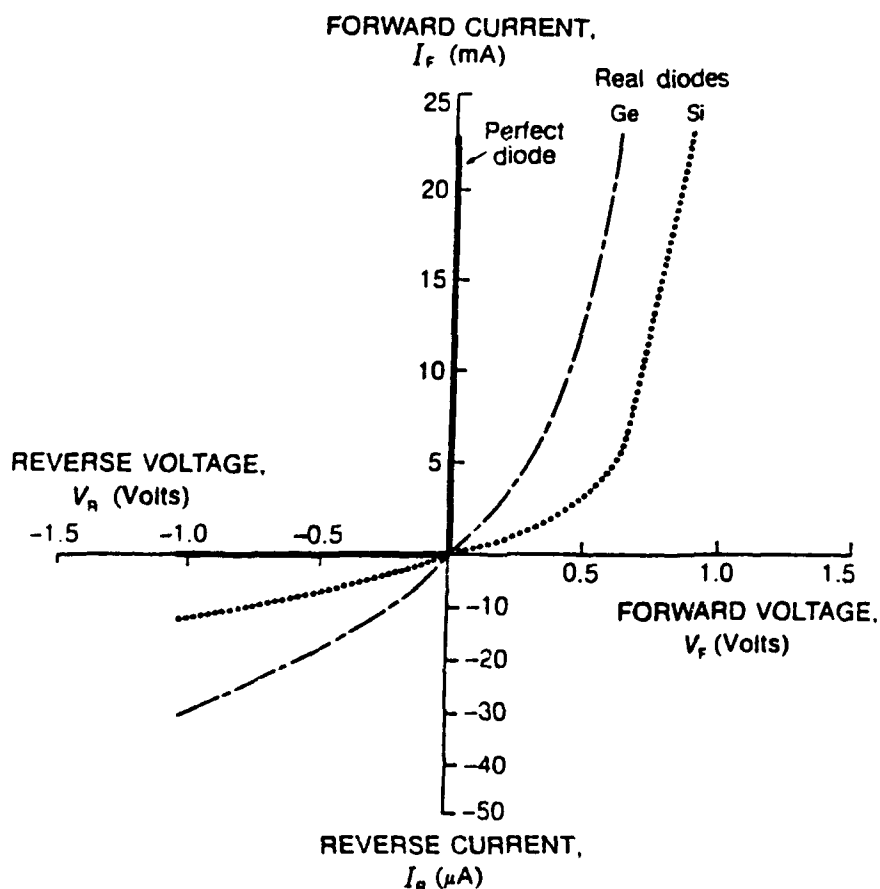


Figure 34. Typical I-V Characteristic Curve for Diodes

(Reference: A. James Diefenderfer, Principles of Electronic Instrumentation, 2nd Ed., Saunders Publishing Co., Philadelphia, PA (1979), pg. 115.)

without loss to the liquid crystal layer. The liquid crystal molecules have reached an optimum orientation by the time this effect occurs and thus any additional voltage drop across the liquid crystal layer does not significantly alter the molecular orientation due to their physical constraint within the cell. This regime results in a saturated response of the modulated read beam. Any increase in write light illumination does not alter the modulated read beam response. The data shown in Figure 16 supports the above arguments. As the frequency of the driving waveform is altered, the impedance, and thus the response, of the LCLV is not significantly altered.

Figure 17 shows the response of the LCLV to variation in write light intensity for discrete driving waveform amplitudes. The above arguments support this data with the following additional explanation. The saturated response of the liquid crystal layer is dependent on the voltage dropped across the entire device. As the overall voltage is decreased, the amount of voltage dropped across the liquid crystal layer is also decreased. The voltage dropped across the photodiode arrangement essentially remains constant for given write light intensities regardless of the field across the entire device. Therefore, the amount of voltage dropped across the liquid crystal is decreased as the overall driving waveform amplitude is decreased. For decreasing voltages across the liquid crystal, the molecular tilt is reduced from the homeotropic alignment that would ideally result in a dark on-state. The molecules still reach a saturated level of operation where any additional write light illumination results in slightly more voltage being dropped across the liquid crystal as opposed to the photosensor. However, this additional voltage is not enough to overcome the molecular forces that confine the molecules to their physically constrained cell. Therefore, for a given driving waveform amplitude, a saturated region of liquid crystal modulation is still observed. Furthermore, the amount of voltage dropped across the liquid crystal is decreased as the device's driving amplitude is decreased. This decreased voltage drop results in saturation of the modulated read beam. Furthermore, the slope of the response approaching the saturated regime is less for decreased driving amplitudes.

B. GEC-Marconi SLM

The response of the GEC-Marconi SLM was detailed in Section V. Essentially, the GEC-Marconi SLM equivalent circuit and behavior may be explained by the same arguments presented above for the Hughes LCLV. The key difference between the Hughes LCLV and GEC-Marconi SLM is the material used for the photodiode. The GEC-Marconi SLM utilized hydrogenated amorphous silicon for the photosensor, whereas the Hughes LCLV utilized cadmium sulfide. Both SLMs utilized a twisted nematic liquid crystal structure. The arguments presented above for the Hughes LCLV are equally valid for the GEC-Marconi SLM. The response of the GEC-Marconi SLM to variations in driving waveform frequency and amplitude is similar to the Hughes LCLV. The GEC-Marconi response time measurements, presented in Section III, verify the modelling of the liquid crystal layer as a parallel RC circuit. The decay and rise times are characteristic of an RC circuit being capacitively discharged and charged. The GEC-Marconi SLM appears to have a response to write light illumination which is not independent of the driving waveform frequency. This characteristic may be explained by the presence of circuit impedance changes, specifically the capacitance effects of the amorphous silicon photodiode. Again, the nematic liquid crystal is believed to have more voltage dropped across it as the write light illumination is increased. This results in an increase in the modulated read beam output until saturation, where the molecules have become physically constrained by the cell and an exorbitant amount of voltage would be necessary to cause any further tilt of the molecules. Therefore, the molecules have reached a maximum angle of tilt and any further voltage applied across the cell will not alter the modulated read beam output.

C. Optically-Addressed Ferroelectric Liquid Crystal SLM

Figure 35 depicts an equivalent electrical circuit for an optically addressed FLC SLM [30]. The circuit is similar to the one developed for the optically addressed twisted nematic liquid crystal (TNLC) SLMs, such as Hughes LCLV and the GEC-Marconi SLM. However, the analysis is different because the TNLC SLMs are driven with ac voltages having frequencies greater than $1/\tau_{\text{relaxation}}$ [25]. The response of a TNLC to an applied electric field is usually fast compared to the relaxation time, back to the state of uniform twist (90 degree twist for the Hughes LCLV and the GEC-Marconi SLM). Beyond the threshold voltage, the applied field induces a dielectric polarization which is proportional to the field, and a torque which is proportional to the square of the applied field. The direction of the torque is independent of the polarity of the electric field because of the field-squared dependence. TNLCs are typically driven with an ac electric field to avoid the buildup of diffused charge at the interfaces. This applied ac field is of a frequency greater than the reciprocal of the response time. When this field is terminated, the liquid crystal relaxes to its uniform twisted state with a relaxation time of

$$\tau_{\text{relaxation}} = \frac{\eta d^2}{\pi^2 K} \quad (2)$$

where η is the viscosity, d is the liquid crystal thickness, and K is an elastic constant [31]. Relaxation times for cells 2-5 microns thick are typically on the order of 1-5 milliseconds.

Before discussion of the equivalent circuit shown in Figure 35, the ideal response of an optically addressed FLC SLM should prove insightful. In the ideal case the FLC SLM circuit may be viewed as a photodiode in series with a capacitor. The photodiode and capacitor represent the photosensor and the FLC, respectively [30]. A periodic waveform such as a square wave may be applied to this circuit at the photosensor, with the liquid crystal being grounded. When a positive voltage is applied, the photodiode becomes forward biased and all the voltage drops across the FLC. This condition switches the FLC to an "off" state. The write light illumination does not affect the state of the liquid crystal during the forward biasing of the diode. The photodiode is reverse biased by the application of a negative voltage. During reverse bias, the current flow is blocked so that the voltage across the FLC remains unchanged. However, current flows when write light illuminates the photodiode, thus charging the FLC to a negative voltage and turning it on. This negative voltage is maintained across the FLC until the drive voltage becomes positive again, which switches the liquid crystal off.

The real components of the optically addressed FLC SLM are not as simple as diodes and capacitors; therefore, the response is not ideal and a more equivalent circuit model must be developed. The parallel RC circuit shown in the lower section of Figure 35 represents the surface stabilized FLC. The parallel resistance (R_{FLC}) is typically large, greater than $20 \text{ M}\Omega\text{-cm}^2$, so that it may be ignored in most analyses. The capacitance of the FLC is composed of two components: One is a physical cell geometry component and the second is a component from the rotation of the liquid crystal molecules. The total capacitance is given as: [30]

$$C_{\text{FLC}} = \frac{\epsilon_0 \epsilon_{\text{FLC}}}{d} + \frac{2P}{\Delta V_{\text{LC}}} \quad (3)$$

where ϵ_0 is the free-space permittivity, ϵ_{FLC} is the relative permittivity of a surface stabilized FLC, d is the FLC cell thickness, P is the ferroelectric polarization, and ΔV_{LC} is the change in voltage across the FLC. The first term is due to cell geometry and the second term is the component due to

rotation of the molecules. The second component is proportional to the ferroelectric polarization, P , such that a charge of $2P$ is switched when the molecules are rotated. For most commercially available Smectic C FLCs, the second component of equation (3) is the dominant factor.

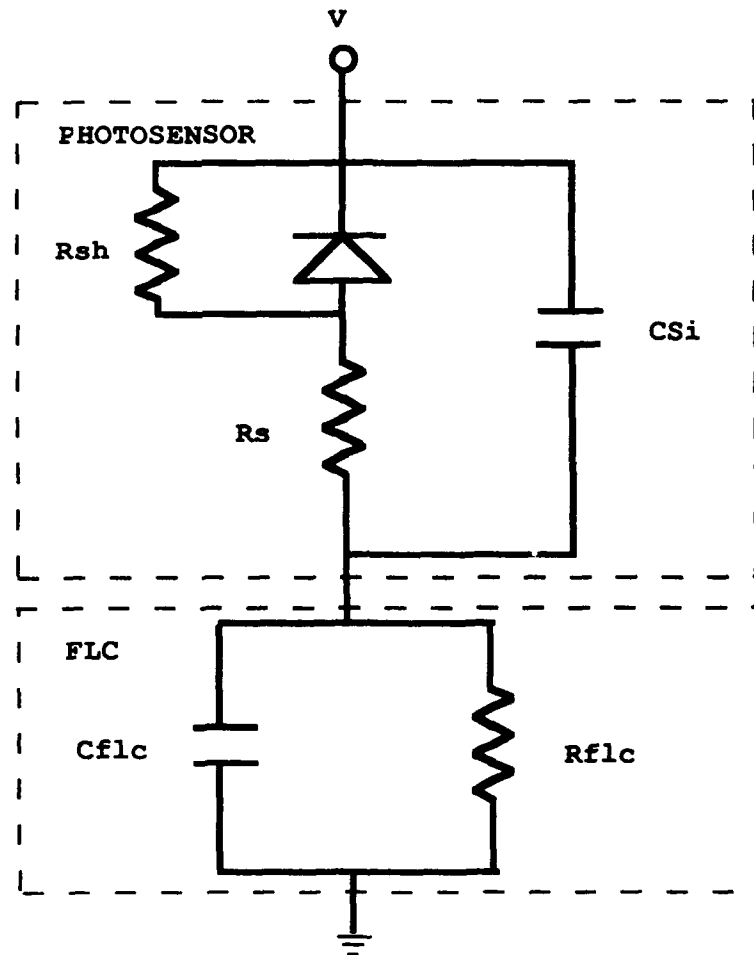


Figure 35. Circuit Model of a FLC SLM

The photosensor is represented in the upper section of Figure 35. The capacitance of the photodiode is dominated by a geometric component defined as [30]:

$$C_{Si} = \frac{\epsilon_0 \epsilon_{Si}}{d_{Si}} \quad (4)$$

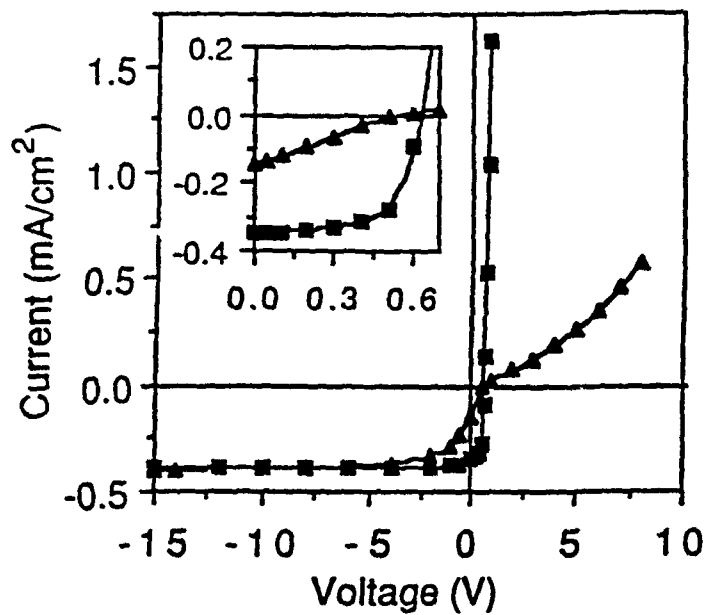
where ϵ_{Si} is the relative permittivity of amorphous silicon and d_{Si} is the thickness. R_s is the series resistance resulting from the electrode sheet resistance and the a-Si:H bulk resistance, and R_{sh} is the shunt resistance. The I-V characteristics of the photodiodes are shown in Figure 36 for two photodiodes under illumination and in the dark, respectively [32]. R_s increases greatly as the thickness of the a-Si:H increases and R_{sh} is a function of the quality of the blocking contacts. For indium tin oxide/a-Si:H barriers, it is sufficiently high at room temperatures [33]. The equivalent

circuit assumes no dielectric mirror or reflector in the SLM. This condition was satisfied for the FLC modulator investigated in this report.

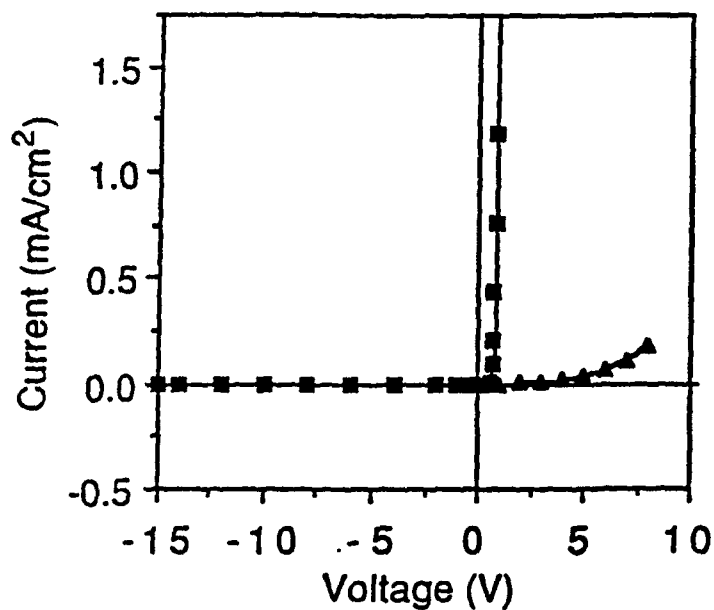
The response of the optically addressed FLC SLM is discussed in detail in Section VI. This behavior is markedly different from the Hughes LCLV and the GEC-Marconi SLM discussed in Sections IV-V. The significant material difference between the Hughes LCLV and the GEC-Marconi SLM with respect to the FLC SLM is the FLC layer. The FLC material is arranged in a surface stabilized geometry (refer to Figure 37). The theory of operation of the FLC SLM is described below.

In the early 1970s, Meyer predicted and demonstrated that chiral Smectic C phase of liquid crystals was ferroelectric [34]. This means that the material can exhibit a macroscopic spontaneous polarization. However, bulk Smectic C phase materials also exhibit a helical order. The spontaneous polarization due to the ordering of molecules per layer yielded a net polarization of zero after transversing through the helical structure. In 1980, Clark and Lagerwall proposed the Surface Stabilized Ferroelectric Liquid Crystal (SSFLC) cell which would unwind the helix and harness the macroscopic polarization [35]. This geometry (shown in Figure 37) consists of a thin layer ($\approx 1.5 \mu\text{m}$) of FLC material sandwiched between two glass electrodes. The helix is spontaneously and permanently unwound due to surface interactions between the FLC and glass plates. Furthermore, the molecules are constrained to move about a tilt cone, shown in Figure 37, by these same surface interactions. For a tilt angle θ the molecules have two stable states, separated by 2θ , which lie in a plane normal to the layers of liquid crystal. A surface charge of $2P$, where P is the ferroelectric polarization, is required to switch the molecules from one state to the other. The two surface stabilized states possess equal energy in the absence of applied fields. However, in the presence of an electric field E , one of the states becomes preferred and the molecules will "flip" about the tilt cone to align the polarization P in the direction of E .

The operation of surface stabilized FLC SLMs is inherently a binary process. If a voltage sufficient to rotate the polarization by twice the tilt angle θ is present, the FLC SLM responds in a manner similar to that shown in Figure 29 where the peak-to-peak voltage was 24 V. The sigmoid shape of the curve is characteristic of a binary response where the intermediate modulation values are due to spatial averaging of binary domains. This sigmoidal curve has also been observed by Moddel [36]. Some of Moddel's data is shown in Figure 38 for different temperature states and FLC structures. If the voltage is other than that voltage which is sufficient to rotate the polarization of the tuned cell by twice the tilt angle, the device does not respond to changes in write light illumination. Figure 30 depicts several voltages which were not sufficient to rotate the molecules and thus the polarization of the light incident on the FLC SLM. Peak-to-peak voltages from 20 to 25 V in 1 V increments were used. The response of all the field amplitudes chosen, with the exception of the optimal 24 V case, was essentially the same. The differences in response curves may be attributed to errors in the experimental measurements. There is some response as a function of write light intensity for this data. This response may be attributed to an averaging of the molecule's rotation near the center of the SLM where the localized field may be strong enough to rotate a few of the molecules.



(a)



(b)

Figure 36. I-V Characteristics for a-Si:H Photodiodes: ■: 2 μm a-Si:H; ▲: 4 μm a-Si:H.
 (a) Under 1 mW/cm^2 Red-Light Illumination, and (b) in the Dark

(Reference: Personal memo from Dr. Garrett Modell, University of Colorado-Boulder.)

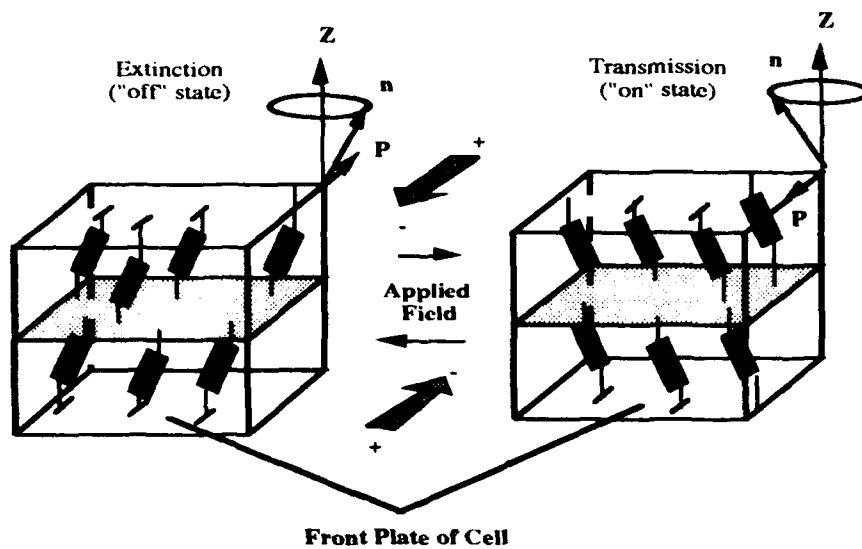


Figure 37. Surface Stabilized Ferroelectric Liquid Crystal (SSFLC) Cell Geometry

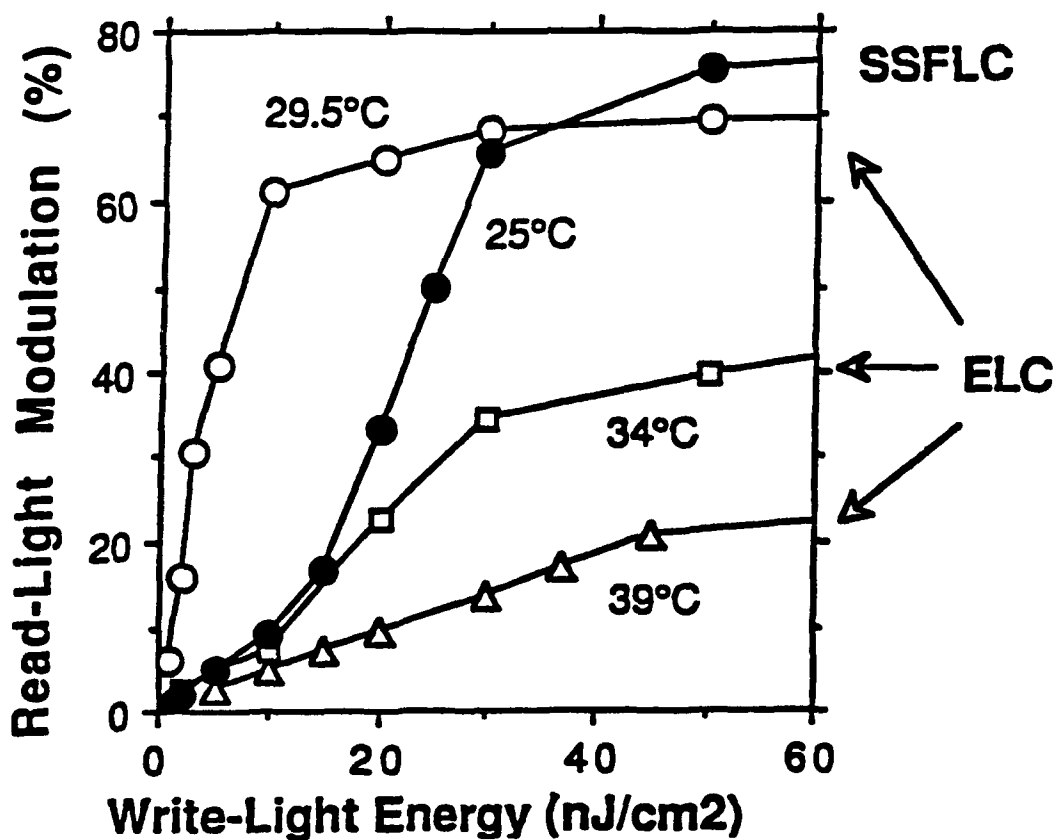


Figure 38. SSFLC Read Light Modulation as a Function of Write Light Intensity for Different Temperatures
(Reference: Personal memo from Dr. Garrett Moddel, University of Colorado-Boulder.)

VIII. CONCLUSION

The preceding sections of this report outlined the results of a series of experiments performed with three types of spatial light modulators: the Hughes LCLV, the GEC-Marconi SLM, and the optically addressed FLC SLM fabricated by the University of Colorado-Boulder. The experimental data collected includes resolution, visibility, and response time measurements of each SLM.

The response of the amplitude modulated read beam as a function of write light intensity was measured for varying drive parameters (amplitude and frequency) of each SLM. The response of the modulated read beam of the Hughes LCLV was also measured for two read light wavelengths (514.5 and 632.8 nm). Each modulator was essentially treated as an engineering "black box." The output of the "black box" was measured as a function of inputs to the "black box." The output of the "black box" was the amplitude modulated read beam intensity and the inputs included electrical driving signal amplitude and frequency, and the write light intensity. An equivalent circuit model for each modulator was developed from the resultant data and presented in Section VII. Future research should include the use of circuit analysis software, such as SPICE, to determine resistance and capacitance values for the models presented in Section VII that most closely approximates the response data presented in Sections IV-VI. Further research of the candidate SLMs should also include a more thorough analysis of the SLM response based on a physical model of the interaction of photons and molecular structures of the devices.

Javidi has proposed the use of nonlinear transformations and nonlinear techniques in the Fourier domain of optical processors for optical image processing applications [8-10]. These proposals have included the use of a high contrast optically addressed SLM in the Fourier plane of a Joint Transform Correlator (JTC) [9]. Computer simulations have shown that the nonlinear input-output characteristics of an optically addressed SLM may significantly improve the correlation signal-to-noise ratio as well as discrimination sensitivity in correlation-based optical pattern recognition architectures [8].

A JTC has an input plane, Fourier plane, and output plane. The input signal and the processing function or reference signal are displayed side by side at the input plane. The joint power spectrum of the input images contains the product of the Fourier transforms of the input and reference signals. Therefore, an inverse Fourier transform of the joint power spectrum can generate a correlation and convolution between the input and reference signals. Figure 39 schematically describes the JTC. Computer simulation and preliminary experimental data have shown that the performance of conventional linear optical processors can be improved by the application of a nonlinear transfer function. The type of nonlinear transformation used in the Fourier domain of these processors depends on the type of operation desired. One proposed application is in a correlator-based pattern recognition system where the image to be detected is located in a scene with large baseband noise. A compression type of nonlinear transformation of the joint power spectrum is useful in obtaining correlations of these types of images in optical correlation due to the low spatial frequency content and signal-like noise present in the background scene. The compression type of transformation is essentially a limiter. The large values of the input are suppressed while the low intensity values of the input to the nonlinear transformer are enhanced. This joint power spectrum transformation emphasizes the fine details of the image that is to be detected. The compression types of nonlinearity have been shown to yield narrower correlation widths, higher peak to sidelobe ratios, and better discrimination sensitivity than conventional correlators.

Preliminary experimental research with a Hughes LCLV in the Fourier plane of a nonlinear joint Fourier transform correlator has validated the computer simulation conclusions [11]. The input-output characteristics of the Hughes LCLV were determined for different driving

frequencies. The input-output characteristic curve of each type of SLM is shown to vary from device to device. Therefore, the characteristic curve must be determined for the specific SLM to be used in a nonlinear optical processor. Javidi's measurement of the input-output characteristic curve of a Hughes LCLV at the University of Connecticut is shown in Figure 40. This particular LCLV was then used in a JTC similar to the one shown in Figure 39. The effects of the LCLV nonlinearity on the JTC performance were tested for three different nonlinear modes of operation of the LCLV corresponding to the three different driving frequencies. The average write light intensity of the input and reference signal joint power spectrum was biased at $1200 \mu\text{W}/\text{cm}^2$. The correlation results are tabulated in Table 3. The correlation peak intensities for the various modes were normalized to the peak intensity obtained by operating the LCLV with a 200 Hz bias frequency. The data verifies that as the slope of the area of operation of the LCLV becomes greater, the nonlinear transformation is more severe, and the correlation performance is thus improved. The more severe the degree of nonlinearity, the more the high spatial frequencies are emphasized, while the intensity of the lower spatial frequency information is suppressed due to SLM saturation effects.

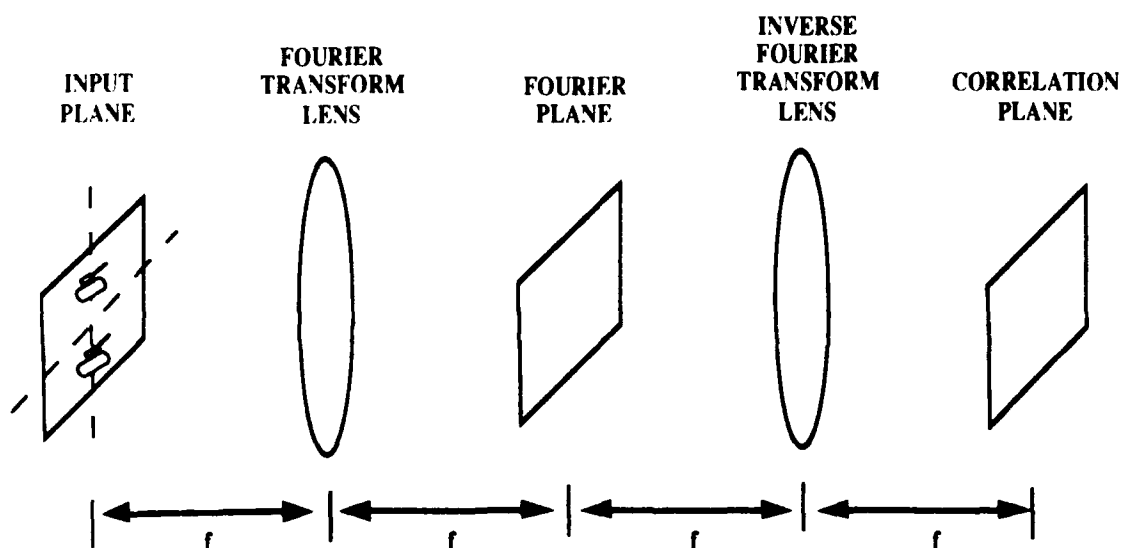


Figure 39. Joint Transform Correlation Architecture

Table 3. Nonlinear Transformation Correlation Results

Tank and tank in the scene noise	Frequency	Peak Intensity	SNR	PSR
	200 Hz	1.0	<1 (false peak)	<1 (false peak)
	120 Hz	1.5	25	3.5
	60 Hz	5.1	35	6.4

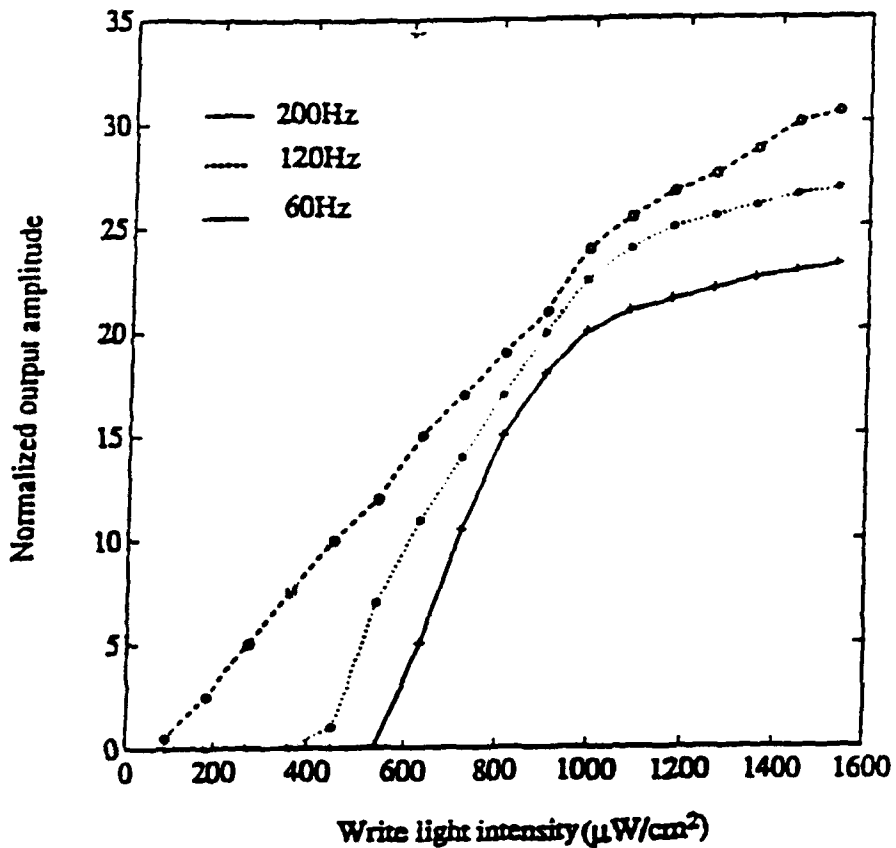


Figure 40. Input-Output Characteristic Curve of Hughes LCLV
From University of Connecticut

The modulated read beam response of the three types of SLMs presented elsewhere within this report should serve as a library of SLM response for nonlinear optical processing techniques proposed in the literature [8-11]. Further research should include the application of the above modulators to nonlinear optical processing architectures. The data presented in this report should serve as a sufficient baseline for these future experiments. The effects of the SLMs on adequate input scene representation as well as Fourier plane nonlinear transformations should be experimentally explored for any optical processor that is being considered for production and implementation in a commercial system.

REFERENCES

1. F. T. S. Yu, S. Jutamulia, T. W. Lin, and D. A. Gregory, "Adaptive real-time pattern recognition using a liquid crystal TV based joint transform correlator," *Appl. Opt.*, Vol. 26, pp. 1370-1372 (1987).
2. F. T. S. Yu, S. Jutamulia, and D. A. Gregory, "Optical parallel logic gates using inexpensive liquid-crystal televisions," *Opt. Lett.*, Vol. 12, pp. 1050-1053 (1987).
3. C. Adams, "Optical Signal Processing: Closer to Reality Than Anyone Might Guess," *Military & Aerospace Electronics*, pp. 29-31 (December 1990).
4. Don A. Gregory, James C. Kirsch, and William M. Crowe, "Optical correlator guidance and tracking field tests," *Proceedings of the 1989 IEEE International Conference on Systems, Man, and Cybernetics*, Cambridge, MA, Vol. 89CH2809-2, pp. 645-650 (1989).
5. J. Grinberg, et al., "A new real-time non-coherent to coherent light image converter: The hybrid field effect liquid crystal light valve," *Opt. Eng.*, Vol. 14, pp. 217-223 (1975).
6. W. M. Crowe, and J. C. Kirsch, "Optical correlator guidance technology demonstration," *SPIE Proceedings*, Vol. 938, pp. 29-35 (April 1988).
7. T. D. Hudson and D. A. Gregory, "Nonlinear response of liquid crystal spatial light modulators," *Opt. & Laser Tech.*, Vol. 22, pp. 357-360 (1990).
8. B. Javidi, "Nonlinear Joint Power Spectrum Based Optical Correlation," *Appl. Opt.*, Vol. 28, pp. 2358-2367 (1989).
9. B. Javidi and J. L. Horner, "Multifunction Nonlinear Signal Processor: Deconvolution and Correlation," *Opt. Eng.*, Vol. 28, pp. 837-843 (1989).
10. B. Javidi and J. L. Horner, "Single SLM joint transform correlator," *Appl. Opt.*, Vol. 28, pp. 1027-1032 (1989).
11. B. Javidi, Q. Tang, D. A. Gregory, and T. D. Hudson, "Experiments on nonlinear joint transform correlator using an optically addressed spatial light modulator in the Fourier plane," *Appl. Opt.*, Vol. 30, pp. 1772-1776 (1991).
12. D. A. Gregory, R. D. Juday, J. Sampsel, R. Gale, R. W. Cohn, and S. E. Monroe, Jr., "Optical characteristics of a deformable-mirror spatial light modulator," *Opt. Lett.*, Vol. 13, pp. 10-12 (1988).
13. T. Hara, M. Sugiyama, and Y. Suzuki, "A Spatial Light Modulator," *Adv. in Electronics and Electron Phys.*, Vol. 64B, pp. 637-647 (1985).
14. J. A. Davis, J. Gamlieli, G. W. Bach, "Optical transmission and contrast ratio studies of the magneto-optic spatial light modulator," *Appl. Opt.*, Vol. 27, pp. 5194-5201 (1988).
15. W. Li, R. A. Rice, G. Moddel, L. A. Pagano-Stauffer, and M. Handschy, "Hydrogenated Amorphous-Silicon Photosensor for Optically Addressed High-Speed Spatial Light Modulator," *IEEE Trans. on Elec. Dev.*, Vol. 36, No. 12, pp. 2959-2964 (1989).

16. M. Powell, C. Powles, and J. Bagshaw, "Effects of Read/Write Isolation on the Resolution of the Marconi Spatial Light Modulator," SPIE Proceedings, Vol 936, pp. 68-75 (1988).
17. D. Armitage, "Gray-scale ferroelectric liquid crystal devices," SPIE, Vol. 1257 Liquid Crystal Displays and Applications, pp. 116-124 (1990).
18. J. Grinberg, et al., "A new real-time noncoherent to coherent light image converter: The hybrid field effect liquid crystal light valve," Opt. Eng., Vol. 14, pp. 217-223 (1975).
19. P. R. Ashley, and J. H. Davis, "Amorphous silicon photoconductor in a liquid crystal spatial light modulator," Appl. Opt., Vol. 26, pp. 241-246 (1987).
20. J. S. Patel, and J. W. Goodby, "Properties and Applications of Ferroelectric Liquid Crystals," Opt. Eng., Vol. 26, pp. 373-384 (1987).
21. K. M. Johnson, M. Handschy, and L. A. Pagano-Stauffer, "Optical Computing and Image Processing with Ferroelectric Liquid Crystals," Opt. Eng., Vol. 26, pp. 385-391 (1987).
22. Max Born and Emil Wolf, Principles of Optics, Sixth Edition, p. 267, Pergamon Press, New York, 1980.
23. B. Javidi, "Optical image processing with nonlinear techniques in the Fourier plane," OE Reports, pp. 11-12 (April 1991).
24. P. Ashley, J. Davis, and T. K. Oh, "Liquid crystal spatial light modulator with a transmissive amorphous silicon photoconductor," Appl. Opt., Vol. 27, pp. 1797-1802 (1988).
25. P. Ashley and J. Davis, "Amorphous silicon photoconductor in a liquid crystal spatial light modulator," Appl. Opt., Vol. 26, pp. 241-246 (1987).
26. J. Grinberg, et al., "A new real-time non-coherent light image converter: The hybrid field effect liquid crystal light valve," Opt. Eng., Vol. 14, pp. 217-225 (1975).
27. G. Moddel, K. Johnson, and M. Handschy, "Photoaddressing of high speed liquid crystal spatial light modulator," SPIE Proceedings, Vol. 754, pp. 207-213 (1987)
28. J. Grinberg, et al., "A new real-time noncoherent light image converter: The hybrid field effect liquid crystal light valve," Opt. Eng., Vol. 14, pg. 218 (1975).
29. A. James Diefenderfer, Principles of Electronic Instrumentation, 2nd ed., Philadelphia: Saunders College Publishing, 1979, pg. 115.
30. W. Li, R. A. Rice, G. Moddel, L. A. Pagano-Stauffer, and M. A. Handschy, "Hydrogenated amorphous-silicon photosensor for optically addressed high-speed spatial light modulator," IEEE Trans. on Elec. Dev., Vol. 36, pp. 2959-2964 (1989).
31. P. G. deGennes, The Physics of Liquid Crystals, Oxford: Clarendon Press, 1974.
32. Personal communication and memo with Dr. Garrett Moddel and Bruce Landreth, University of Colorado-Boulder.
33. B. Drevillon, et al., "In Situ Investigation of the Optoelectronic Properties of Transparent Conducting Oxide/Amorphous Silicon Interfaces," Appl. Phys. Lett., Vol. 54, pp. 2088-2090 (1989).

34. R. B. Meyer, L. Liebert, L. Strzelecki, and P. Keller, "Ferroelectric Liquid Crystals," *J. de Physique*, Vol. 36, pp. L69-L71 (1975).
35. N. A. Clark and S. T. Lagerwall, "Submicroseconds bistable electro-optic switching in liquid crystals," *Appl. Phys. Lett.*, Vol. 36, pp. 899-901 (1980).
36. B. Landreth, C. C. Mao, and G. Moddel, "Operating Characteristics of Optically Addressed Spatial Light Modulators Incorporating Distorted Helix Ferroelectric Liquid Crystals," to be published in *Japanese Journal of Applied Physics*, Vol. 30 (1991); personal memo from Bruce Landreth, University of Colorado-Boulder.

LIST OF SYMBOLS

ac	alternating current
A/D	analog to digital
a-Si:H	hydrogenated amorphous silicon
BS1, BS2, BS3	beamsplitters
CCD	charge-coupled device
C_d	capacitance of the diode
CdS	cadmium sulfide
CdTe	cadmium telluride
C_{lc}	capacitance of liquid crystal
C_m	capacitance of dielectric mirror
d	thickness of liquid crystal
DC	direct current
d_{Si}	thickness of hydrogenated amorphous silicon
ΔV_{lc}	change in voltage across the liquid crystal
D1, D2	photodetectors
E	electric field
ϵ_0	free-space permittivity
ϵ_{flc}	relative permittivity of ferroelectric liquid crystal
ϵ_{Si}	relative permittivity of amorphous silicon
FLC	ferroelectric liquid crystal
Ge	germanium
HeNe	helium neon
Hz	unit of frequency (Hertz)
I_{min}	minimum light intensity
I_{max}	maximum light intensity
I_r	read light intensity
I_w	write light intensity
I-V	current-voltage relationship
JTC	joint transform correlator
K	elastic constant
KHz	measure of frequency (kilohertz)
λ	wavelength
$\lambda/2$	one-half wavelength
$\lambda/4$	one-quarter wavelength
$\lambda/10$	one-tenth wavelength
LCLV	liquid crystal light valve
lp/mm	unit of resolution (line pairs per millimeter)
L1, L2, L3	lenses
LR1, LR2	lenses within the read beam
μm	unit of measure (micron)
$\mu W/cm^2$	unit of power density (microwatts per square centimeter)
$M\Omega\text{-}cm^2$	sheet resistance

LIST OF SYMBOLS (cont'd)

$\mu\text{W}/\text{cm}^2$	unit of power density (milliwatts per square centimeter)
mm	unit of measure (millimeter)
msec	unit of time (millisecond)
MTF	modulation transfer function
v	visibility
η	viscosity
nm	unit of measure (nanometer)
NRC	Newport Research Corporation
P	ferroelectric polarization
P1, P2, P3	Polarizers
π	Pi
PSR	peak to sidelobe ratio
RC	resistor-capacitor
R_{td}	backward resistance of diode
R_{fd}	forward resistance of diode
R_{flc}	resistance of ferroelectric liquid crystal
R_{lc}	resistance of liquid crystal
R_{m}	resistance of dielectric mirror
R_{s}	series resistance
R_{sh}	shunt resistance
Si	silicon
SLM	spatial light modulator
SNR	signal to noise ratio
SSFLC	surface stabilized ferroelectric liquid crystal
θ	angle (theta)
TNLC	twisted nematic liquid crystal
$\tau_{\text{relaxation}}$	relaxation time of liquid crystal
USAF	United States Air Force
V	Volt
VBS	variable beamsplitter
$V_{\text{p-p}}$	peak-to-peak voltage
$-V_{\text{p}}$	negative peak voltage

DISTRIBUTION

	<u>Copies</u>
Director U.S. Army Research Office ATTN: SLCRO-PH P. O. Box 12211 Research Triangle Park, NC 27709-2211	1
Headquarters Department of the Army ATTN: DAMA-ARR Washington, DC 20310-0623	1
Headquarters OUSD&E ATTN: Ted Berlincourt The Pentagon Washington, DC 20310-0623	1
ITT Research Institute ATTN: GACIAC 10 W. 35th Street Chicago, IL 60616	1
U. S. Army Materiel System Analysis Activity ATTN: AMXSY-MP (Herbert Cohen) Aberdeen Proving Ground, MD 21005	1
Department of Electrical Engineering Pennsylvania State University ATTN: Dr. F. T. S. Yu University Park, PA 16802	1
Department of Physics The University of North Carolina at Charlotte ATTN: Dr. Eddy C. Tam Charlotte, NC 28223	1
Department of the Air Force Rome Labs ATTN: ESOP/Dr. Joe Horner Hanscom AFB, MA 01731-5000	1
Dean, College of Science University of Alabama in Huntsville Materials Science Bldg, Room C207 Huntsville, AL 35899	1

Dist-1

DISTRIBUTION (cont'd)

	<u>Copies</u>
Dr. William H. Carter Naval Research Laboratory, Code 8304 Washington, DC 20375	1
Dr. W. T. Cathey 228 Alpine Way Boulder, CO 80304	1
Dr. Arthur Chiou Rockwell International, MS A25A P.O. Box 1085 Thousand Oaks, CA 91358	1
Dr. John D. Downie NASA Ames Research Center Intelligent Systems Technology Branch, MS 244-4 Moffett Field, CA 94035	1
Dr. Marvin D. Drake The Mitre Corporation, MS E050 Burlington Road Bedford, MA 01730	1
Dr. F. Trevor Gamble Denison University Department of Physics Granville, OH 43023	1
Dr. Bahram Javidi University of Connecticut Electrical Engineering Department 260 Glennbrook Road, U-157 Storrs, CT 06269-3157	1
Dr. Sing H. Lee University of California, San Diego 9500 Gilman Drive, ECE Dept. La Jolla, CA 92093-0407	1
Dr. Freddie Liu Physical Optics Corporation 20600 Gramercy Place, Suite 103 Torrance, CA 90501	1

DISTRIBUTION (cont'd)

	<u>Copies</u>
Dr. Hau-Kuang Liu JPL/Caltech Mail Stop 303-310 Pasadena, CA 91109-8099	1
Dr. Michael V. Morelli Texas Tech University Optical Systems Lab Department of Electrical Engineering Lubbock, TX 79409-4439	1
Dr. Dennis R. Pape Photonic Systems Inc. 1800 Penn St., Suite 4B Melbourne, FL 32901	1
Dr. Bernard H. Soffer Hughes Research Labs 3011 Malibu Canyon Road, RL 68 Malibu, CA 90265	1
Dr. Wilfrid B. Veldkamp MIT Lincoln Labs 244 Wood St., L-270 Lexington, MA 02173	1
Mr. Carl Verber Georgia Institute of Technology Atlanta, GA 30307	1
Dr. John F. Walkup Texas Tech University Department of Electrical Engineering P. O. Box 4439 Lubbock, TX 79409-3102	1
Dr. Shudong Wu Pennsylvania State University Electrical Engineering Department University Park, PA 16802	1
Dr. Xiangyang Yang Pennsylvania State University Electrical Engineering Department University Park, PA 16802	1

DISTRIBUTION (cont'd)

	<u>Copies</u>
AMSMI-RD	1
AMSMI-RD-CS-T	1
AMSMI-RD-CS-R	15
AMSMI-GC-IP, Fred Bush	1
AMSMI-RD-WS, W. Wharton	1
J. Bennett	1
S. Troglen	1
AMSMI-RD-WS-PO, Tracy D. Hudson	50
Don A. Gregory	1